HYDRODYNAMICS OF CONTAINED OIL SLICKS

by

ROBERT J. VAN HOUTEN

B.S. Webb Institute of Naval Architecture
(1968)
M.S. George Washington University
(1971)

SUBMITTED IN PARTIAL FULFILLMENT

OF THE REQUIREMENTS FOR THE

DEGREE OF

DOCTOR OF PHILOSOPHY

at the

MASSACHUSETTS INSTITUTE OF TECHNOLOGY

September, 1976

Signature of Author. . . . . .
Department of Ocean Engineering, September, 1976

Certified by . . . . . .
Thesis Supervisor

Accepted by. . . . . .
Chairman, Departmental Committee on Graduate Students

HYDRODYNAMICS OF CONTAINED OIL SLICKS

by

ROBERT J. VAN HOUTEN

Submitted to the Department of Ocean Engineering, September 1976, in partial fulfillment of the requirements for the degree of Doctor of Philosophy.

ABSTRACT

As a first step in understanding the instabilities which are observed when oil is contained in the presence of a shear flow, the problem of finding the mean shape of a pool of oil in front of a barrier moving in water of infinite depth is considered. The author presents experimental evidence that this problem is one of a gravity current in which no head loss takes place outside of a relatively thin boundary layer, and that irrotational flow theory can be used in the water phase. The oil phase is considered to be hydrostatic. An equilibrium equation is developed which balances frictional, dynamic, and hydrostatic forces. A Green's function approach is used, in which the slick is assumed to be slender. Flow quantities are expressed as a perturbation series in terms of integrals of an assumed friction coefficient and lower order solutions. Numerical solutions are presented for several assumed friction distributions. The problem of non-uniform convergence near the leading edge is considered, and possible approaches toward obtaining an inner expansion valid there are discussed.

Thesis Supervisor: Professor Jerome H. Milgram
Title: Associate Professor of Naval Architecture

ACKNOWLEDGEMENTS

The author wishes to express his gratitude to Professor Jerome H. Milgram, who first aroused his interest in the hydrodynamic problems of oil containment and provided guidance in the preparation of this thesis.

Credit is also due Professors Ole S. Madsen and Justin E. Kerwin for their contributions as thesis committee members, and Mrs. Deborah Schmitt, who prepared the manuscript.

TABLE OF CONTENTS

LIST OF FIGURES

LIST OF FIGURES (continued)

LIST OF SYMBOLS

A	constant in leading edge potential
a	arbitrary parameter in conformal mapping; constant in Taylor series of C_f
B_{ij}	coefficient of term in expansion of perturbation pressure
b	coefficient of x in C_f Taylor series
C, $C(x)$	integration constant
C	constant in conformal mapping
C_f	coefficient of friction
C_f^*	reduced coefficient of friction of 0(1)
C_D	drag coefficient
C_P	phase velocity
c	coefficient of x^2 in C_f Taylor series
D	depth of free surface of oil-water interface beneath stagnation level (units of $U^2/2g$)
d	characteristic depth of headwave; coefficient of x^3 in C_f Taylor series
F_{ij}	fictitious slick depth associated with i,j^{th} kinematic condition
$f(x)$	general function of x
g	gravitational acceleration
h	height (depth) of gravity current above (below) rigid boundary (undisturbed free surface)
h_∞	asymptotic mean value of h
k	wave number
k_{cr}	critical wave number for instability
ℓ	characteristic length scale of headwave

M_{ij}	coefficient of i,j^{th} term in expansion of m
M_{eig}	eigenfunction for M_{ij}
m	depth of oil slick beneath undisturbed free surface
n	exponent in leading edge potential
P	pressure
Re	Reynolds number
$S = U^3/\Delta g\nu$	square of Froude number based on diffusion length
T_{aw}, T_{ao}, T_{ow}	surface tension (a-air, w-water, o-oil)
t	thickness of oil slick
U	free stream velocity
U_{cr}	critical value of U for instability
u	perturbation velocity in x direction
V	local flow speed
v	perturbation velocity in y direction
We	Weber number
w	complex velocity u-iv
x	horizontal dimension in physical plane
y	vertical dimension in physical plane
z	complex position vector x+iy
z_{bp}	location of branch point
α	angle at which free surface approaches stagnation point
β	argument of A
γ	slenderness parameter

$\Delta[\ ]$ change in value of bracketed quantity

$\Delta = (\rho_w - \rho_o)/\rho_w$ relative density ratio

δ thickness of slick before containment

ζ position vector in mapped plane

θ argument of z

μ_o dynamic viscosity of oil

ν_o kinematic viscosity of oil

ν_w kinematic viscosity of water

ξ integration variable

ρ_H density of heavier fluid

ρ_L density of lighter fluid

ρ_o density of oil

ρ_w density of water

σ frequency

τ interfacial stress

ϕ complex or real velocity potential

ϕ_{ij} coefficient of i,j^{th} term in expansion of ϕ

ϕ_{LE} complex velocity potential in leading edge region

$\nabla^2 = \frac{\partial^2}{\partial x^2} + \frac{\partial^2}{\partial y^2}$ 2-D Laplace operator

$\nabla = \frac{\partial}{\partial x}\hat{i} + \frac{\partial}{\partial y}\hat{j}$ 2-D gradient

$[\ ]'$ non-dimensional quantity; derivative

$[\ ]_{ij}$ i,j^{th} term of expansion of bracketed quantity
i = order of γ, j = order of Δ

$[\ ]_x, [\ ]_y$ partial derivatives of bracketed quantities

I. INTRODUCTION

In recent years, the large scale of ocean-borne transport and offshore production of petroleum has increased significantly the danger to the natural environment presented by the spillage of oil at sea. In an effort to reduce the impact of spills once they occur, there have been numerous attempts to design effective oil collection equipment. A general feature of this equipment is increased efficiency when operated in deeper oil pools. The most effective means of concentrating a relatively thin slick for ease in collecting is to drag through it a floating barrier which extends some way above and below the free surface. A number of hydrodynamic problems resulting in the leakage of oil past such a barrier have been encountered. Although those problems dealing with the design of the barrier itself have largely been solved, there remains a problem which is independent of barrier design, and which appears to be fundamental to the concept of oil containment in the presence of a shear flow. At the leading edge of the oil pool thickened by the barrier there is formed a lump or, as it is called, a headwave. At velocities on the order of a half knot, oil droplets are torn off the lee side of this headwave, and depending on their size and make-up either rise to the slick or flow beneath the barrier. For reasons as yet imperfectly understood, those

rising to the slick are slow to rejoin, and a significant portion of them are swept under the barrier. The extent of this entrainment of oil increases with towing velocity, and it is virtually impossible to collect oil at speeds greater than one knot.

The purpose of this thesis is to present a theory by which the steady-state configuration of oil in front of a barrier can be analyzed. This is a first step in understanding the nature of the instability which results in entrainment. In Chapter II, past work in the field will be reviewed. Chapter III contains the derivation of the equilibrium equation and presents experimental evidence justifying the assumptions made. The boundary value problem is posed. A perturbation scheme for the solution of this problem is presented in Chapter IV, and some results are given. In Chapter V, the leading edge geometry is discussed, with a view toward developing an inner expansion which might be matched to that developed in Chapter IV. Chapter VI contains a discussion of the results and recommendations for further work. Some other approaches to the problem are discussed in Appendices 1-5, and a short description of experimental procedures is contained in Appendix 6.

II. HISTORY OF THE PROBLEM

Classical Work

The class of problems in which the present one falls is that of gravity, or density, currents. This class consists of flows of one fluid above or beneath another due to a density difference between them. Naturally occurring examples are the movement of a meteorological cold front, the intrusion of a saline wedge under the fresher water of an estuary (or conversely, the run-off of fresh river water over denser sea water), turbidity currents under clear water, and avalanches of snow-laden air. Interest in these problems led to analyses of the problem of gravity currents which predated the present interest in oil spill clean-up.

Von Kármán (1940) considered a layer of heavy fluid (of density ρ_H) intruding with velocity U along a solid horizontal boundary into a lighter fluid (ρ_L) of infinite extent. He adopted a frame of reference moving with the propagation velocity, and assumed that the heavy fluid was hydrostatic, and the lighter fluid inviscid. Matching pressure on the interface, and using Bernoulli's equation, he obtained the relationship:

$$\frac{V^2}{2g} - \frac{\rho_H - \rho_L}{\rho_L} h = 0 \qquad \text{(II.1)}$$

where V is the local velocity and h is the height of the interface. By looking for a "corner flow" where the velocity squared varies linearly with distance from the stagnation point, von Kármán showed that at the leading edge the interface makes an angle of 60° with the boundary. He stated that it could be shown that a head must exist which extends significantly higher than the mean asymptotic height of:

$$h_\infty = \frac{\rho_L}{\rho_H - \rho_L} \frac{U^2}{2g} \qquad \text{(II.2)}$$

Although von Kármán did not present his reasoning, one can see that the reduced pressures away from the stagnation region which causes the drag on a semi-infinite half-body to be zero (Prandtl and Tietjens, 1934) would cause a headwave in a gravity current which acts as von Kármán postulates.

The model gravity current proposed by von Kármán is shown in Figure II.1. Numerous investigators, notably Keulegan (1958) and Middleton (1966), have reported experimental observations of currents resembling that postulated by von Kármán, although in practice the leading edge appears rounded. Von Kármán attributes this to bottom friction.

Benjamin (1968) argued that the assumption of irrotational flow was inconsistent with the assumption of constant intrusion speed. There is a net hydrostatic driving force

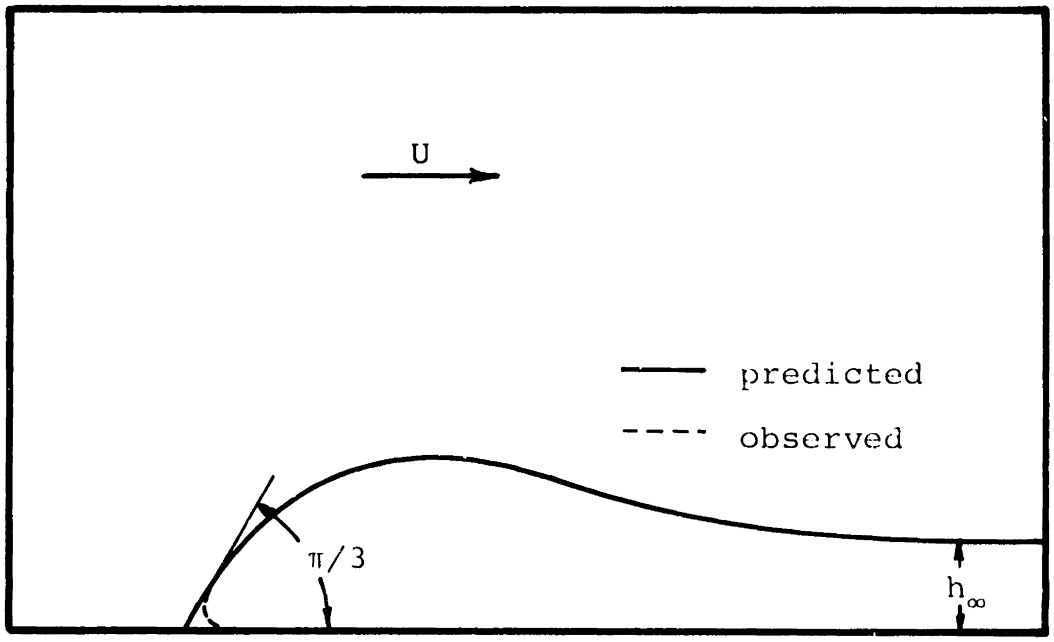

Figure II.1 Classical Gravity Current

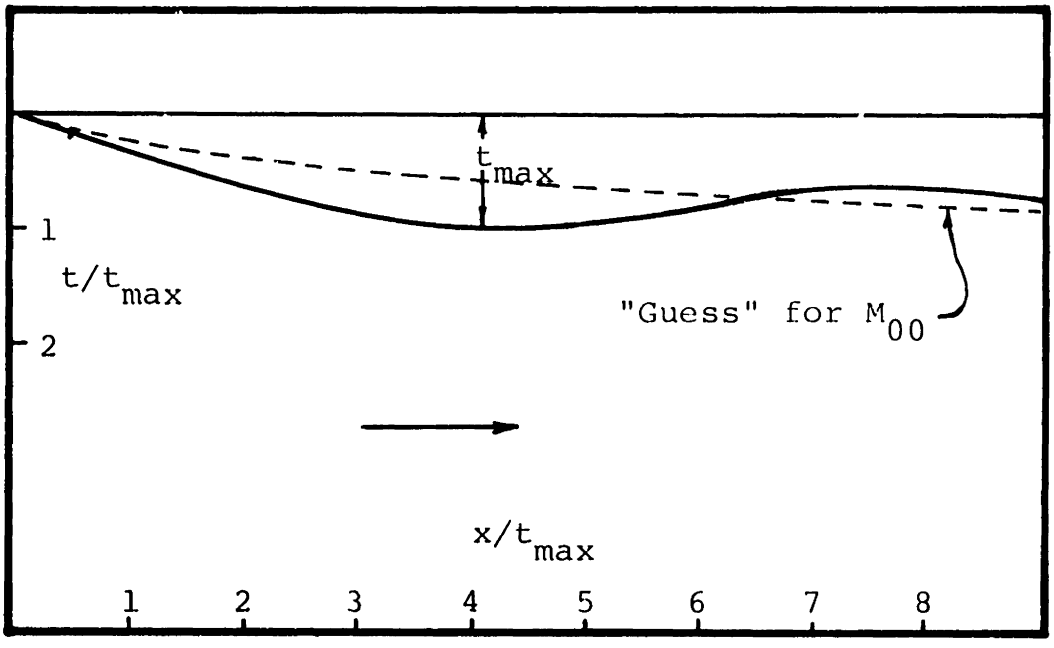

Figure II.2 Typical Headwave Geometry as Reported by Miller

of $(gh_\infty^2/2)(\rho_H - \rho_L)$, and since in irrotational flow there is no frictional drag, and no hydrodynamic drag on a semi-infinite half-body, this force cannot be balanced. Benjamin showed that the necessary drag force could not be achieved by the wave resistance of interfacial waves, and therefore must be found in a momentum deficiency due to dissipative processes. He mentioned the possible role in some cases of bottom friction in providing a force balance, but stated that in general a wake would form behind a "breaking" headwave. Benjamin showed that von Kármán's result for asymptotic height could be arrived at without using Bernoulli's equation, due to the fact that wakes exhibit constant piezometric pressure far downstream.

Benjamin did not consider the possibility that the dissipative phenomena necessary to balance the hydrostatic driving force behind a gravity current could be limited to a thin interfacial boundary layer. The work was in general concerned with cavity flows, which of course cannot support shear stress on the interface. If a boundary layer did exist, gravity currents could still be investigated using irrotational flow theory. Von Kármán's analysis would still be in error, however, due to the fact that the pressure within the current would no longer be independent of distance behind the leading edge, and an asymptotic level would not

be reached.

Although the aforementioned work was directed at the problem of a gravity current moving along a rigid boundary, the ideas can easily be applied to gravity currents on a free surface. In this case, if one makes the same assumptions as did von Kármán, he finds the asymptotic depth of the slick to be undetermined by the pressure condition, which merely states that the asymptotic thickness of the upper fluid must be ρ_H/ρ_L times the asymptotic depth of the interface below the undisturbed free surface, h_∞. The hydrostatic motive force is now $(\rho_H/\rho_L)(gh_\infty^2/2)(\rho_H - \rho_L)$. There is still the necessity for momentum deficit to balance this force.

Prandtl (1952) also looked at the problem of gravity currents, specifically the initial motion of a heavy fluid beneath a lighter one, as might occur after partially raising a vertical sluice gate which initially separated the two fluids. Ignoring hydrostatic effects, and assuming both fluids to be inviscid, he calculated the rate of advance of the front from the requirement for pressure continuity at the interface. He thus envisioned a flow in which the heavy fluid moved toward the front at a velocity greater than the intrusion velocity and thereafter rolling up in a vortex. Benjamin envisioned his model for a steadily advancing gravity current to be the natural development of Prandtl's model for

the initial flow, the breaking headwave evolving from the turbulence caused by the re-entrainment of the heavy fluid originally deflected upwards.

There are alternative initial value problems, however, which can also lead to a steady-state gravity current; specifically the problem of towing a barrier through an oil slick, initially very thin. One conceivable steady flow for this problem is one where the oil remains very thin, moving with the velocity of the barrier, with the water stationary under it, except in the neighborhood of the barrier itself. This flow would indeed satisfy the conditions one can impose on a frictionless fluid. However, if the fluid is real, large frictional forces would be generated by such a long slick moving with respect to the water. This frictional force would build up the slick until it (and dynamic forces which would exist once the slick became thick) was balanced by hydrostatic forces. Benjamin's model, where hydrostatic forces outweigh any interfacial friction, clearly would not apply here, since friction is the active force working to build up an oil slick. Thus we find that the classical analyses of gravity current phenomena are really insufficient to deal with oil slicks. Although von Kármán's model is inappropriate for a frictionally-restrained current, his method of analysis - the use of Bernoulli's equation in the

upper fluid - should still be useful, and Benjamin's objections should not apply.

Recent Work

One of the earliest investigators to address specifically the dynamics of contained oil slicks was Wicks (1969), who reported experimental results and developed a theoretical model. He reported the existence of a headwave at the leading edge of the oil, and the entrainment of oil drops off the leeward side. He attributed this entrainment to the inherent instability of the headwave reported by Benjamin. He treated the portion of the slick aft of the headwave as a region where viscous and hydrostatic forces were balanced:

$$\tau = \rho_o g \frac{\rho_w - \rho_o}{\rho_w} t \frac{dt}{dx} \qquad \text{(II.3)}$$

where ρ_o and ρ_w are the densities of oil and water, respectively, t is the oil thickness, and τ the interfacial shear stress.

Hoult (1970) applied this friction-hydrostatic balance to the entire slick, and reported that experimental observations indicated that slicks grow parabolically. From the rate of this growth, he deduced the value of the (constant) skin friction.

Comprehensive experiments on contained oil slicks at Hydronautics, Inc. were reported by Lindenmuth, Miller, and Hsu (1970) and Miller, Lindenmuth, Lehr, and Abrahams (1972). These reports showed photographs of representative slicks, and reported the interfacial instability and droplet entrainment mentioned by Wicks. They presented a sketch of typical headwave geometry (Figure II.2), and reported that the densiometric Froude number based on headwave depth decreased with speed, from about 1.46 at 1 fps to 1.0 at 2 fps. They attributed this effect to the larger Weber numbers at the higher speeds. The earlier report stated that the headwave Froude number decreased to .95 at 1 fps for SAE30 motor oil. The theoretical model presented for build-up behind the headwave was the same as that of Wicks and Hoult.

Benjamin's analysis of gravity currents in an infinitely deep fluid was a relatively small part of a discussion mainly concerned with gravity currents (modelled, in the absence of viscosity, as cavity flows) in fluids with depths small with respect to the lengths of the currents (cavities). The flow was considered to be uniform far downstream. Benjamin found that for energy-conserving flow the depth of the current was one half the total depth of the fluid (modified somewhat if the upper surface were free). Lesser depths resulted in energy dissipation, whereas greater depths

required an external source of energy. The maximum Froude number based on propagation speed and channel depth was found to occur for an energy-dissipating flow. In 1972 Wilkinson extended this part of Benjamin's work to the case of oil slicks in shallow water. Although he recognized the importance of frictional forces on long slicks, he stated that they were unimportant forward of 20 "slick thicknesses" downstream, basing his arguments on the implicit assumption of a friction coefficient of .01 and a drag coefficient of two. Were the more realistic value of $C_d = .1$ used, Wilkinson's arguments would lead to the conclusion that viscous forces were unimportant forward of one slick thickness downstream, and were he to consider that the friction coefficient might be significantly higher than .01 near the leading edge, he would be forced to conclude that friction and dynamic forces might be comparable in the leading edge region. Wilkinson then made the assumption of uniform flow in the channel at the end of this upstream region, and more or less repeated the Benjamin analysis. He thereby found the equilibrium depth of the "dynamic" region of a contained oil slick as a function of flow speed, depth of water, and density of oil, as well as a critical containment speed as a function of water depth and oil density. He then extended his results to the case of deep water, retrieving the von Kármán - Benjamin

result of (II.2). Wilkinson somewhat ingenuously pointed out that for this case the assumption of uniform flow became "rather tenuous", but supported this result as conforming to experimental data. In his treatment of the "viscous zone" of an oil slick, he included dynamic effects, but once again used the uniform flow approximation. He again extended his results to deep water, obtaining for that case the Wicks-Hoult result. A 1973 paper considered the critical depth, and corresponding critical length, of the viscous zone. Although as noted above the separation of a dynamic region from the rest of the slick seems unjustified, Wilkinson's treatment of the viscous zone seems to be valid for sufficiently small water depths. His extension of the shallow water theory to the deep-water case, which more accurately describes actual clean-up operations, seems completely unjustified.

The most comprehensive set of experiments performed to date on contained oil slicks were those reported by Hale, Norton, and Rodenberger (1974). They measured headwaves for various oils at different flow speeds and obtained results similar to those of Lindenmuth. They numerically sought a correlation between densiometric Froude number based on headwave thickness and Weber and Reynolds numbers (the latter based on oil viscosity). They found strong Weber effects, but weak Reynolds number dependence. One cannot, however, draw

the conclusion that frictional forces are unimportant in the development of the headwave. The least viscous oil investigated was still four times as viscous as water. The velocity of the interface would therefore be a small percentage of the free stream velocity for all cases investigated, and the boundary layer in the water would not differ significantly. One might expect to see a greater Reynolds number effect were it based on water viscosity. At higher flow speeds this Reynolds number becomes larger at a given densiometric Froude length, so the build-up of the headwave (measured in Froude units) can be expected to be less rapid than in the case of lower flow speeds. This effect would seem to counteract the Weber number dependence reported by both Lindenmuth and Hale. The influence of surface tension on the set-up of oil will be discussed in Chapter III.

Hale also published some mean velocity profiles in the headwave region. The profiles taken in the "neck" behind the headwave do not indicate the existence of a separated flow. Unfortunately, they did not include any turbulence data, which might help confirm this observation.

Zalosh (1974) presented a numerical solution for headwave development and entrainment. He ignored hydrostatic terms and frictional forces. He justified the latter omission by referencing the weak Reynolds number dependence of headwave

geometry found by Hale. As pointed out above, this is of course unjustified, as is the neglect of hydrostatic terms. Zalosh modelled the headwave with a set of discrete vortices along the air-water, air-oil, and oil-water interfaces. An original configuration which did not exhibit headwave properties was allowed to move due to local induced velocities. A headwave developed, and eventually the local curvature behind it became large. A criterion was selected, based on an assumed value of Weber number, by which regions of high curvature were cut off from the rest of the slick and allowed to move as an entrained two-dimensional oil bubble. At large times, the numerical scheme became unstable, and a steady-state entrainment model was not achieved.

Leibovich (1976) argued that the instability mechanism in the neighborhood of the headwave (as well as elsewhere) was that of non-linear Kelvin-Helmholtz waves. He presented the linear theory for these waves in a horizontal oil slick of finite thickness with no friction, but with surface tension at both the water-oil and oil-air interfaces. Jones (1972) had made a similar analysis, but had neglected surface tension in the oil-air interface. Leibovich showed that the critical Kelvin-Helmholtz speed was significantly lower than that reported for entrainment. He quoted the work of Drazin (1970) who found that for two semi-infinite parallel streams

non-linear effects served to equilibrate waves which were unstable according to the linear theory. At the velocities at which Lindenmuth (1970) reported droplet entrainment, Drazin's theory predicted equilibrated wave slopes of about unity. Leibovich stated that the headwave was the most unstable portion of the oil slick simply because the local current speed was maximum there. He estimated the increase in current speed to be approximately 40 percent, and hypothesized that at a speed 40 percent higher than that at which entrainment began at the headwave there would be entrainment from all parts of the slick. The headwave would still be the region where the entrainment process was most vigorous. The significance of this work should not be underestimated. Previous investigators had generally attributed headwave instability to the fundamental instability first reported by Benjamin (or, according to one's perspective, by Prandtl). The flow over the lee side of the headwave was assumed to be separated, with large fluctuations of pressure, giving rise to energy dissipation in both phases in this region. Although some authors mentioned Kelvin-Helmholtz instability, none postulated tnat it was the sole cause of headwave instability. If this is the case, the steady-state set-up of oil which determines the environment in which the small-scale instability manifests itself can be investigated using the powerful tools

of irrotational flow theory.

The problem of spatially growing waves on an oil slick was investigated by Milgram and Van Houten (1974). The dispersion relation (ignoring, as did Jones, the air-oil surface tension) was numerically solved for wave numbers corresponding to various real frequencies. All values of density ratio, Weber number, and Froude number investigated were found to admit of imaginary wave numbers. Briggs (1964), however, showed that the proper criterion for spatial instability in initial value problems is the existence of solutions to the dispersion relationship which have real wavenumber and imaginary frequency, as found by Jones and later corrected by Leibovich. Milgram and Van Houten also presented some elements of the present work.

III. THE EQUILIBRIUM EQUATION AND BOUNDARY VALUE PROBLEM

In developing an equilibrium equation, various assumptions were made. Among them are: a) two-dimensionality, b) steadiness, c) smallness of surface tension forces, d) slenderness of the slick, e) hydrostatic pressure distribution in the oil phase, f) smallness of momentum flux in the oil phase, and g) irrotational flow in the water phase outside of a thin boundary layer. These will be taken up in turn, and where necessary justified on the basis of experimental findings. The experiments referred to were conducted in the Precision Flume located in the Ocean Engineering Hydrodynamics Laboratory. Details of the equipment and procedures used are given in Appendix 6.

Two-Dimensionality

In practice, oil containment booms take on the shape of a catenary between mooring points (Milgram, 1971). Headwave phenomena, however, are restricted to a region extending approximately ten densiometric Froude lengths back from the leading edge. For typical flow velocities, this distance is about three feet. The upstream influence of a barrier will be restricted to the area within a distance of about one barrier draft, or two or three feet. Therefore, if one ignores wave effects (which, due to refraction and reflection,

might extend the barrier's influence) the headwave should be uninfluenced by the barrier over most of the extent of this headwave; say over regions of the slick where the slick length exceeds ten feet.

Aerial photographs (Milgram and Van Houten, 1974) have shown that oil lost by entrainment is located near the apex of a deployed barrier. However, it can be assumed that this oil is entrained uniformly across the barrier's length, and is later concentrated near the apex by velocities parallel to the barrier which arise in its near-flow field.

Steady Flow

The actual containment of oil at sea is influenced by unsteady effects of two kinds. The most obvious is the fact that in all but the most sheltered waters ocean waves will be present. Effects due to these waves will be ignored for the very practical reason that they immensely complicate a problem which is already difficult. The model developed will hopefully represent the physics which act when barriers are used in the absence of surface waves. The second source of unsteady effects is due to the fact that even in the absence of these external sources of unsteadiness the oil-water interface is generally unstable. The unsteadiness, however, has a small characteristic length scale, and for the purposes

of modelling the large-scale behavior, it will be assumed that these waves affect that behavior only through their effect on the frictional forces acting on the oil.

Smallness of Surface Tension Forces

The Weber number, or ratio of dynamic to surface-tension forces, can be expressed as $[C_D \rho_w U^2/(T\ d/\ell^2)]$, where C_D is the drag coefficient, and d and ℓ are the characteristic depth and length scales, respectively. The findings of experimental investigators [Lindenmuth (1970), Hale (1974)] are that the headwave depth is approximately $U^2/\Delta g$, and the length is about seven times this. Substituting, one gets $We \simeq 50 C_D \rho U^4/\Delta g T$. This number is typically 1500 or so. Thus, surface tension is not significant when interfacial curvature is as small as that exhibited typically by the mean headwave geometry. However, surface tension is of dominant importance in determining the nature and extent of small-scale instability. Small scale waves, in turn, increase the interfacial friction much as roughness on a rigid boundary. The Weber number dependence of headwave geometry reported by Hale and by Lindenmuth is no doubt due to this mechanism. In developing a model for the mean geometry, the effects of surface tension will be included through an augmented friction coefficient.

Slenderness of Oil Slick

The assumption of slenderness can be made on the basis of observation. Photographs published by Lindenmuth and experimental observations by the present author of typical headwave geometry appear to be qualitatively different from photographs of gravity currents published by von Kármán, Yih (1965), Keulegan, and others. Whereas the latter exhibit leading edges which are round, oil slicks appear to be wedge shaped, with entrance angles of less than 20° and often more like 10°. This difference may be due to either the existence of the free surface or to the importance of friction in the oil slick problem, and will be discussed in Chapter V. In any case, the assumption of slenderness appears to be justified.

Hydrostatic Pressure in Oil

Figure III.1 depicts a typical section of the oil slick. Due to the slender slick approximation the interfacial slope, γ, can be considered small compared with unity. The Navier-Stokes equations are as follows:

$$u \frac{\partial u}{\partial x} + v \frac{\partial u}{\partial y} = -\frac{1}{\rho_o} \frac{\partial P}{\partial x} + \nu_o \left(\frac{\partial^2 u}{\partial x^2} + \frac{\partial^2 u}{\partial y^2}\right) \qquad \text{(III.1)}$$

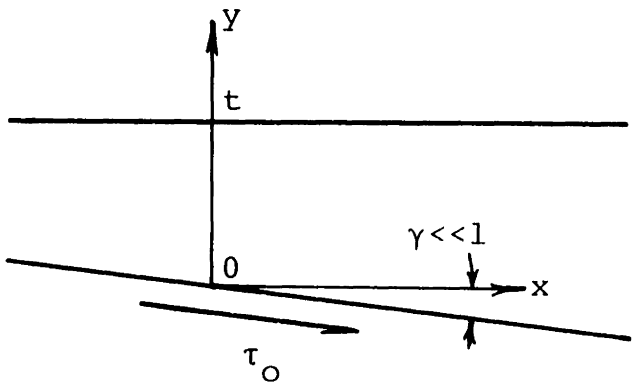

Figure III.1 Section of Oil Slick

$$u \frac{\partial v}{\partial x} + v \frac{\partial v}{\partial y} = -\frac{1}{\rho_o} \frac{\partial P}{\partial y} + \nu_o \left(\frac{\partial^2 v}{\partial x^2} + \frac{\partial^2 v}{\partial y^2}\right) - g \qquad \text{(III.2)}$$

$$\frac{\partial u}{\partial x} + \frac{\partial v}{\partial y} = 0 \qquad \text{(III.3)}$$

Assume that the relevant length scales in the x and y directions are t/γ and t, respectively. Letting primes denote non-dimensional quantities or order unity, $x' = \gamma x/t$ and $y' = y/t$. Equation (III.3) becomes:

$$\frac{\gamma}{t} \frac{\partial u}{\partial x'} + \frac{1}{t} \frac{\partial v}{\partial y'} = 0$$

and one can deduce that $v \simeq 0(\gamma u)$.

The relevant velocity scales in the x and y directions can be taken to be U and γU, respectively. Substituting in (III.1),

$$\frac{U^2\gamma}{t} u' \frac{\partial u'}{\partial x'} + \frac{U^2\gamma}{t} v' \frac{\partial u'}{\partial y'} = -\frac{\gamma}{\rho t} \frac{\partial P}{\partial x'}$$

$$+ \nu_o \left(\frac{\gamma^2 U}{t^2} \frac{\partial^2 u'}{\partial x'^2} + \frac{U}{t^2} \frac{\partial^2 u'}{\partial y'^2}\right)$$

If $\nu_o/U\gamma t >> 1$ (and $\gamma << 1$) acceleration terms can be ignored, leaving the following dimensional x-momentum equation:

$$\frac{\partial P}{\partial x} = \mu \frac{\partial^2 u}{\partial y^2} \qquad \text{(III.4)}$$

Equation (III.2) becomes:

$$\frac{\gamma^2 U^2}{t} u' \frac{\partial v'}{\partial x'} + \frac{\gamma^2 U^2}{t} v' \frac{\partial v'}{\partial y'} = -\frac{1}{\rho t} \frac{\partial P}{\partial y}$$

$$+ \nu_o \left(\frac{\gamma^3 U}{t^2} \frac{\partial^2 v'}{\partial x'^2} + \frac{\gamma U}{t^2} \frac{\partial^2 v'}{\partial y'^2}\right) - g$$

Thus, $\partial P/\partial y + \rho g$, which represents the deviation of the vertical pressure gradient from hydrostatic, is $0(\gamma)$ smaller than $\partial P/\partial x$, or:

$$\frac{\partial P}{\partial y} = -\rho g + 0(\gamma) \frac{\partial P}{\partial x}$$

$$P \simeq -\rho g y + f(x) \qquad \text{(III.5)}$$

To estimate the order of magnitude of U in terms of the local interfacial shear stress τ_o and thickness t, Equation (III.4) can be integrated as follows, using the fact that $\partial P/\partial x$ is not

a function of y:

$$C(x) + \frac{\partial P}{\partial x} y = \mu_o \frac{\partial u}{\partial y}$$

From shear stress continuity at the interface,

$$-\tau_o + \frac{\partial P}{\partial x} y = \mu_o \frac{\partial u}{\partial y}$$

And from shear stress continuity at the free surface,

$$-\tau_o + \frac{\partial P}{\partial x} t = 0$$

$$\frac{\partial P}{\partial x} = \frac{\tau_o}{t} = \rho_o g \frac{\partial}{\partial x} \qquad \text{(height of free surface)}$$

Integrating again,

$$C(x) - \tau_o y + \frac{\tau_o}{2t} y^2 = \mu_o u$$

From continuity:

$$\int_0^t u \, d y = 0$$

$$Ct - \frac{\tau_o t^2}{2} + \frac{\tau_o t^2}{6} = 0$$

$$C = \frac{\tau_o t}{3}$$

$$u = \frac{1}{\mu}\left[\frac{\tau_o t}{3} - \tau_o y + \frac{\tau_o}{2t} y^2\right] \simeq 0\left(\frac{\tau_o t}{\mu}\right)$$

Therefore, the requirement for neglecting advection terms becomes:

$$\frac{\nu_o}{t\gamma u} = \frac{\mu_o^2}{\rho_o t^2 \gamma \tau_o} >> 1$$

A conservative estimate of the typical magnitude of the denominator in the headwave region at a current speed of 1 fps and with a specific gravity of .9 is:

$\rho_o \simeq 2$ slugs/ft^3 $\qquad t \simeq u^2/\Delta g \simeq .33$ ft. $\qquad \gamma \simeq \frac{1}{5}$

$\tau_o \simeq .01$ lb/ft^2 $\qquad \rho_o t^2 \gamma \tau_o = .0004$

Therefore, $\mu_o^2/\rho_o t^2 \gamma \tau_o$ will be large (>10) for oil of viscosity greater than .06 slugs/ft-sec., or 3000 centipoise. This is

somewhat more viscous than an SAE 140 oil, which is a significantly heavier oil than that typically spilled. At a lower current speed of .5 fps, t and τ_o are each reduced by a factor of 4, so that the denominator is reduced by a factor of 64. The viscosity necessary for advection terms to be small is now 400cp, or somewhere between a 30 and 40 weight oil.

The justification for using the hydrostatic assumption is a) that it significantly simplifies the analysis, and b) that Hale found that headwave depth varied as $Re^{-.016}$ for oils ranging from No. 2 Diesel (μ = 3.9cp) to SAE40 (μ = 565cp). This means that over this range of viscosities, headwave depths varied approximately 8 percent. One might assume, therefore, that deviations from the assumed hydrostatic pressure distribution do not produce any qualitative differences in headwave geometry.

Neglect of Momentum Flux in Oil

The rate of change of momentum in the oil, per unit length of slick, is:

$$\frac{d}{dx}\int_0^t \rho u^2 dy \simeq 0\left(\frac{\rho_o \tau_o{}^2 t^2 \gamma}{\mu_o{}^2}\right)$$

It is thus smaller than τ_o by a factor on the order of $\mu_o{}^2/\rho_o\tau_o t^2\gamma$. Thus the assumption of no momentum flux within

the oil is entirely consistent with that of a hydrostatic pressure distribution. In the case where oil of thickness δ is being collected at the leading edge of a contained slick, this assumption is no longer valid except for very small δ, since the incoming momentum flux is $\rho_o \delta U^2$.

Irrotational Flow in Water Phase

It was shown in Chapter II that there appears to be no fundamental requirement for flow separation behind the headwave. Early arguments based on unbalanced hydrostatic forces cannot apply to a gravity current which builds up due to frictional forces. Furthermore, the observed instability is not necessarily one involving head loss. However, there is conversely no fundamental reason why the flow must remain attached, and one must rely on experimental observations.

Hale published velocity profiles for both Diesel #2 and SAE 30 oils in currents of about 1 fps. No significant region of separated flow was apparent. In an experiment conducted by the author, a wooden form was constructed to model the mean shape of a 150cp oil of specific gravity .921 in a current of .94 fps. This form was placed in a current of the same speed, and a velocity survey made in the neighborhood of the headwave. The results for mean flow are shown in Figure III.2. At section C, where the boundary layer was largest, the mean

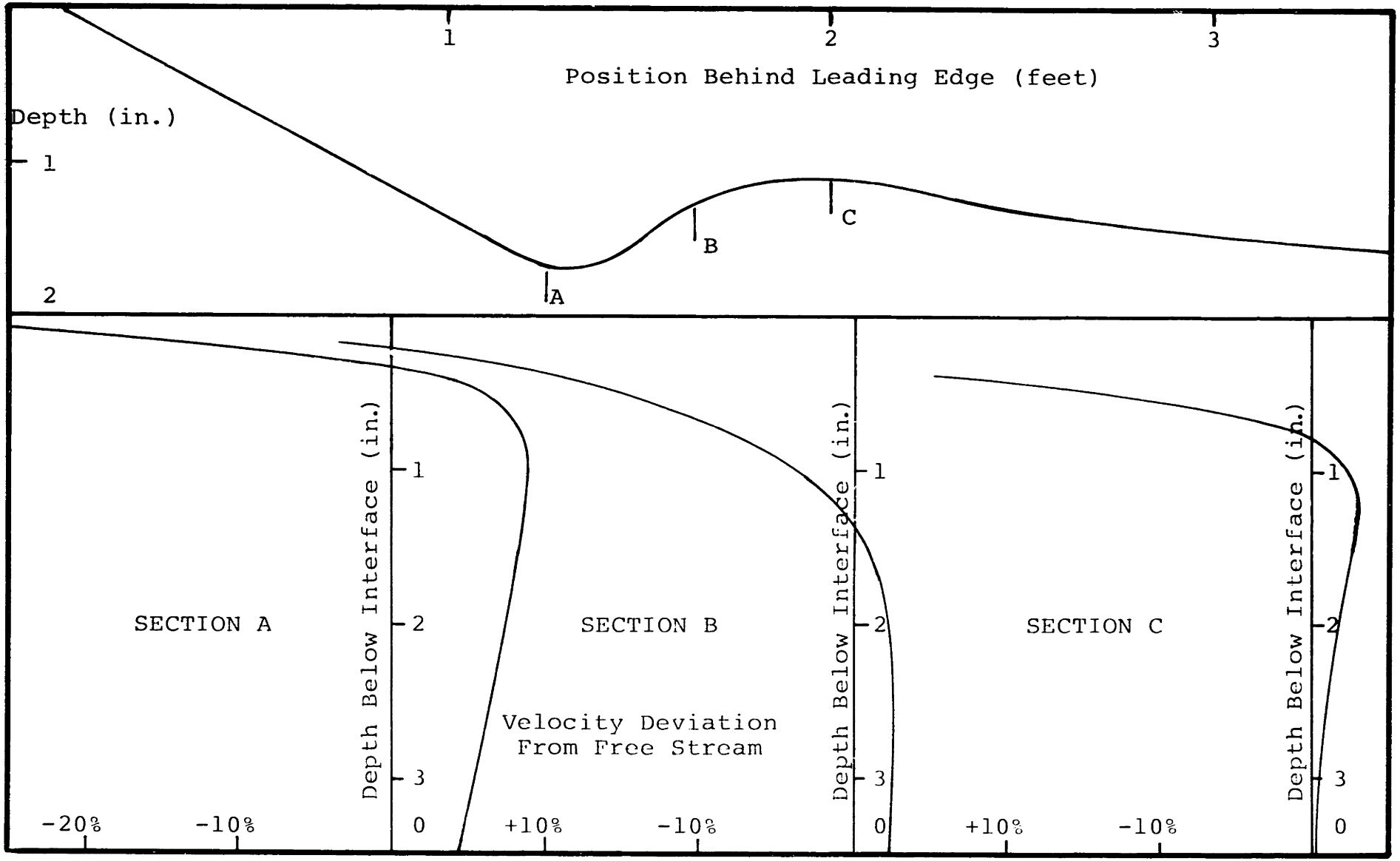

Figure III.2 Velocities in Region Behind "Rigid" Headwave

flow was diminished by 15% at a distance of 83% of the headwave depth from the local interface, 41% at 42% headwave depth, and 57% at 21% of the headwave depth. It appears that no actual separation is taking place. Although turbulence measurements were attempted, no reliable results were obtained due to the interference of the convection noise of the hot film annemometer.

The nature of the interfacial instability in the region of the headwave was discussed in Chapter II. Although earlier authors assumed that the instability was caused by fluctuating pressures in the separated region behind a headwave, Leibovich presented arguments that it was of the Kelvin-Helmholtz type. If this is the case, the instability should appear as relatively long-crested waves, and measurable wave characteristics should agree with those predicted by Kelvin-Helmholtz theory. Lamb (1932) gives expressions for the dispersion relationship, the most critical wave number, and the critical velocity for linear Kelvin-Helmholtz instability. For the present problem, these are:

$$C_P = \frac{\sigma}{k} = -\frac{U\rho_w}{\rho_w + \rho_o}$$

$$\pm \sqrt{\frac{(\rho_w - \rho_o)g/k + T_{ow}k}{\rho_w + \rho_o} - U^2 \frac{\rho_w \rho_o}{(\rho_w + \rho_o)^2}} \qquad \text{(III.7)}$$

$$k_{cr} = \sqrt{\frac{(\rho_w - \rho_o)g}{T_{ow}}} \qquad \text{(III.8)}$$

$$U_{cr} = \left[2 \frac{\rho_w + \rho_o}{\rho_w \rho_o} \left[(\rho_w - \rho_o) g T_{ow} \right]^{1/2} \right]^{1/2} \qquad \text{(III.9)}$$

It can be seen that all unstable waves in a particular oil move at a particular percentage of free stream speed.

The author measured the wave number and phase velocity of the interfacial waves in the headwave region for a typical oil and obtained the results shown in Figure III.3. It can be seen that the observed phase velocities agree quite well with those predicted by the theory and the observed wave numbers lie in the unstable region. At velocities significantly larger than the critical velocity, the observed wave numbers are less than the critical wavenumber. This is no doubt due to non-linear effects. One can conclude from the data that headwave instability is, indeed, of the Kelvin-Helmholtz type. Thus, the "breaking" of the headwave would appear not to involve head loss in the flow.

It should also be pointed out that should there be a separated region of the flow over the headwave, this separation should be due to the existence of a strongly adverse pressure gradient in an irrotational flow solution to the contained oil

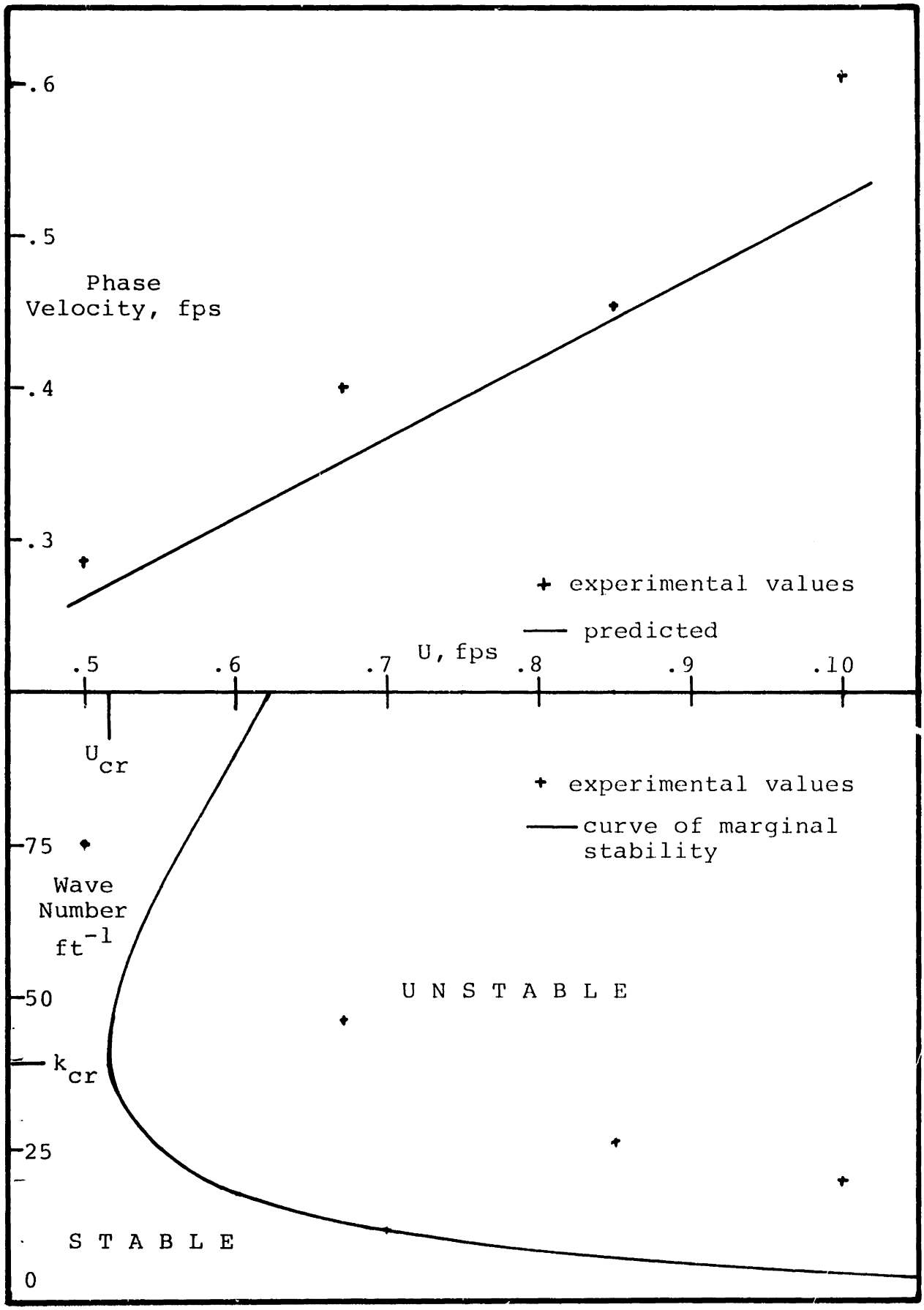

Figure III.3 Phase Velocity and Wavenumber of Headwave Instability

slick problem. Thus, the assumption of irrotational flow should lead to a solution which will serve to verify (or not, as the case may be) the original assumption.

The Equilibrium Equation

Figure III.4 shows a section of an oil slick and the forces acting on it. These forces are a) hydrostatic pressure, b) frictional shear force, and c) dynamic pressure in the water phase which, for irrotational flow, can be calculated from Bernoulli's equation. Since the momentum flux in the oil will be ignored, the horizontal forces acting on the oil can be equated:

$$\frac{1}{2}\rho_o g t^2 + (m + \frac{\Delta m}{2})\Delta m \rho_w g - \Delta m \rho_w \frac{(V^2 - U^2)}{2}$$

$$+ \frac{\rho_w}{2} C_f U^2 \Delta x = \frac{1}{2}\rho_o g (t + \Delta t)^2 \qquad \text{(III.10)}$$

Letting Δx become arbitrarily small, this equation reduces to:

$$\rho_w g\, m \frac{dm}{dx} - \rho_w \frac{V^2 - U^2}{2}\frac{dm}{dx} + \frac{\rho_w}{2} C_f V^2 = \rho_o g t \frac{dt}{dx} \qquad \text{(III.11)}$$

In the absence of surface tension, the pressure must be constant

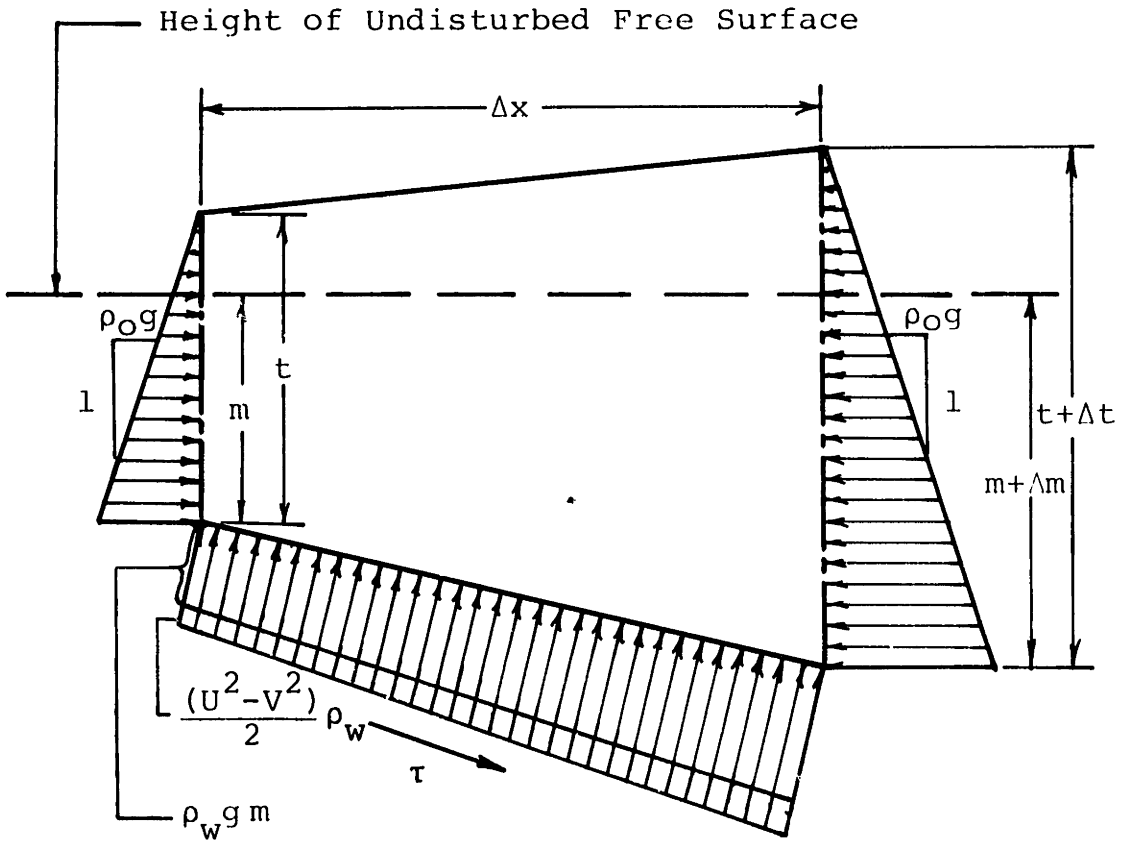

Figure III.4 Forces Acting on Slick Element

across the interface. Assuming a hydrostatic pressure distribution in the oil, this relationship can be written:

$$\rho_o gt = \rho_w gm - \frac{\rho_w}{2} (V^2 - U^2) \qquad \text{(III.12)}$$

Differentiating,

$$\rho_o g \frac{dt}{dx} = \rho_w g \frac{dm}{dx} - \rho_w VV_x \qquad \text{(III.13)}$$

Substituting (III.12) and (III.13) into (III.11), one gets:

$$\Delta m \frac{dm}{dx} - \frac{\Delta}{2g} (V^2 - U^2)\frac{dm}{dx} - \frac{1}{g} m VV_x + \frac{1}{2g^2} (V^2 - U^2) VV_x$$

$$= \frac{1-\Delta}{2g} V^2 C_f \qquad \text{(III.14)}$$

where Δ now represents the relative density difference $(\rho_w - \rho_o)/\rho_w$. This is the dimensional form of the equilibrium equation, and in factored form is:

$$(m - \frac{V^2 - U^2}{2g})(\Delta \frac{dm}{dx} - \frac{VV_x}{g}) = \frac{(1-\Delta)}{2g} V^2 C_f \qquad \text{(III.15)}$$

This is the dynamic boundary condition which applies on the oil-water interface.

It should be noted that if Equation (III.15) is written as:

$$[F_1][\frac{d}{dx} F_2] = \frac{1-\Delta}{2g} V^2 C_f$$

F_1 is simply $1/\rho_w g$ times the pressure at the interface. The solution to $F_1=0$, $\substack{-\infty < x < +\infty \\ y = -m}$, would be a steady water wave. F_1=constant would correspond to a uniform layer of oil superposed on the water. Similarly, F_2 is $1/\rho_w g$ times the interfacial pressure for a fluid with a density equal to $\rho_w - \rho_o$, or equivalently, the pressure drop across the interface for water flowing under a semi-infinite hydrostatic fluid. The solution to $F_2=0$, $\substack{-\infty < x < +\infty \\ y = -m}$, would once again be a steady "water" wave, but with $k = \sigma^2/\Delta g$. In general, one would expect the present problem to contain wave-like solutions as $x \to \infty$. The water wave solution mentioned above could exist with any value of shear stress, but the interfacial wave can exist only if the shear stress vanishes.

The dynamic boundary condition on the free surface in front of the oil slick is just $F_1=0$, or

$$m - \frac{(V^2 - U^2)}{2g} = 0 \qquad -\infty < x < 0 \qquad y = -m \tag{III.16}$$

where here $y = -m$ represents the free surface.

There are three possible lengths with which to scale m. These are a) U^2/g, b) $U^2/\Delta g$, and c) ν/U. The experimental evidence indicates that the densiometric Froude length -- $U^2/\Delta g$ -- is the correct one for describing headwave phenomena. One might expect the behavior at the leading edge to scale with U^2/g, and the behavior in the bulk of the slick, where dynamic pressures are small, to scale with the Reynolds length, ν/U. The leading edge problem will be considered in Chapter V.

Scaling all lengths with respect to $U^2/\Delta g$, and velocities with respect to U, Equation (III.15) becomes:

$$[m' - \frac{\Delta}{2}(V'^2 - 1)][\frac{dm'}{dx'} - V'V'_{x'}] = \frac{1-\Delta}{2} V'^2 C_f \qquad \text{(III.17)}$$

where primed variables are non-dimensional.

Expressing V' in terms of relative perturbation velocities u and v, one gets:

$$[m - \Delta(u + \frac{u^2}{2} + \frac{v^2}{2})][\frac{dm}{dx} - (u + \frac{u^2}{2} + \frac{v^2}{2})_x]$$

$$= \frac{1-\Delta}{2}(1 + 2u + u^2 + v^2)C_f \qquad \text{(III.18)}$$

where primes have been dropped.

Since the flow is assumed to be irrotational, velocity can be represented as the gradient of a velocity potential $\Phi = x + \phi$, where ϕ is the perturbation potential. Equation (III.18) and the scaled version of (III.16) become:

$$[m - \Delta(\phi_x + \frac{\phi_x^2}{2} + \frac{\phi_y^2}{2})][\frac{dm}{dx} - (\phi_x + \frac{\phi_x^2}{2} + \frac{\phi_y^2}{2})_x]$$

$$= \frac{1-\Delta}{2}(1 - 2\phi_x + \phi_x^2 + \phi_y^2)C_f \qquad \begin{bmatrix} 0 < x < +\infty \\ y = -m \end{bmatrix} \qquad \text{(III.19)}$$

$$m - \Delta(\phi_x + \frac{\phi_x^2}{2} + \frac{\phi_y^2}{2}) = 0 \qquad \begin{bmatrix} -\infty < x < 0 \\ y = -m \end{bmatrix} \qquad \text{(III.20)}$$

The kinematic boundary condition which the potential must obey at the free surface and the oil-water interface is that of no normal velocity:

$$\phi_y = (1 + \phi_x)\frac{dm}{dx} \qquad -\infty < x < +\infty \qquad y = -m \qquad \text{(III.21)}$$

Since the flow is assumed to be incompressible, the governing equation for velocity potential is Laplace's equation:

$$\phi_{xx} + \phi_{yy} = 0$$

Figure III.5 shows the resultant boundary value problem for ϕ. Note that no boundary condition can be applied at $x = +\infty$, since the slick can be expected to continue to grow indefinitely.

Utilizing the assumption of slenderness, the characteristic length scale over which flow quantities change is $(U^2/\Delta g\gamma)$, where γ is the slenderness parameter. Relative perturbation velocities can be assumed to be $0(\gamma)$. When expressed in terms of quantities which are $0(1)$, the dynamic boundary conditions are:

$$[m - \Delta(\gamma\phi_x + \frac{\gamma^2}{2}\phi_x^2 + \frac{\gamma^2}{2}\phi_y^2)][\gamma\frac{dm}{dx} - (\gamma^2\phi_x + \frac{\gamma^3}{2}\phi_x^2 + \frac{\gamma^3}{2}\phi_y^2)_x] = \frac{1-\Delta}{2}(1 + 2\gamma\phi_x + \gamma^2\phi_x^2 + \gamma^2\phi_y^2)C_f \quad \text{(III.22)}$$

$$m - \Delta(\gamma\phi_x + \frac{\gamma^2}{2}\phi_x^2 + \frac{\gamma^2}{2}\phi_y^2) = 0 \quad \text{(III.23)}$$

$$[-\infty < x < 0 \qquad y = -m]$$

and the kinematic condition:

$$\phi_y = (1 - \gamma\phi_x)\frac{dm}{dx} \quad \text{(III.24)}$$

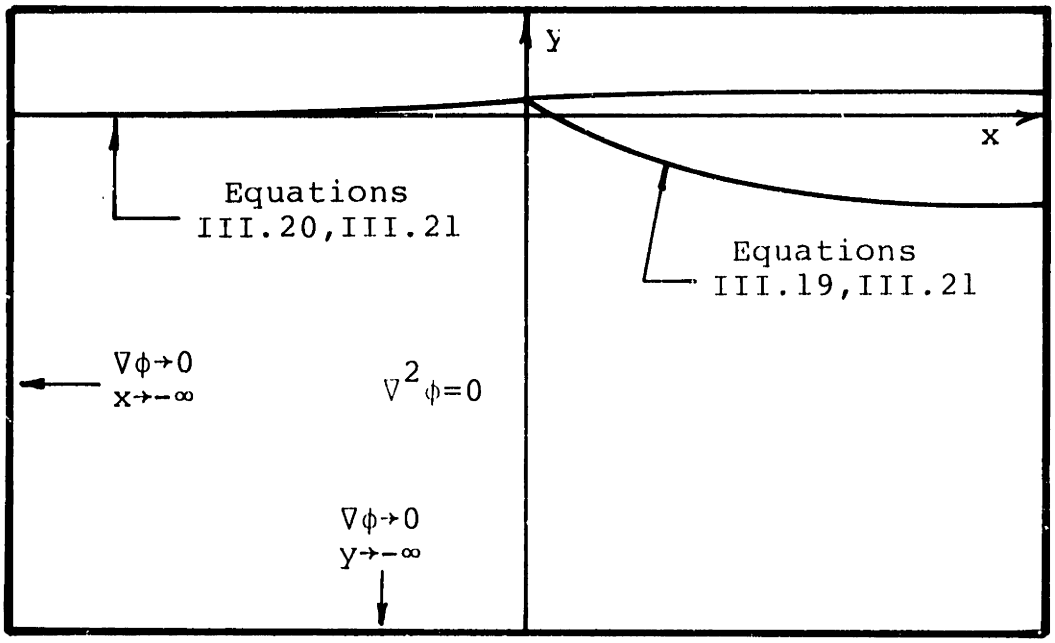

Figure III.5 Boundary Value Problem for Non-Slender Slick

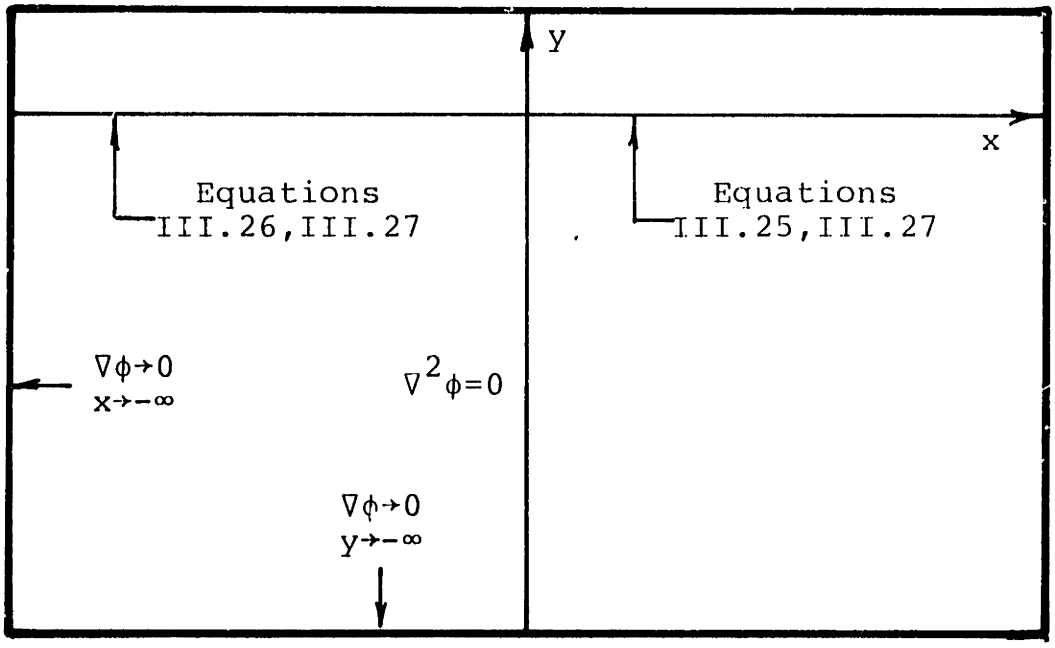

Figure III.6 Boundary Value Problem for Slender Slick

Consistent with this assumption of slenderness is the transfer of the boundary conditions to the x-axis. A Taylor series expansion is used to describe the perturbation potential (and its derivatives) at the interface in terms of its value on the real axis:

$$\phi(x,-m) = \phi(x,0) - m\gamma\phi_y(x,0) + \frac{m^2}{2}\gamma^2\phi_{yy}(x,0) + \ldots$$

The x-derivative of the second factor (F_2) of the interfacial dynamic boundary condition is a total derivative, and the Taylor series expansion must be taken accordingly. These series expansions are substituted in Equations (III.22), (III.23), and (III.24), resulting in the following:

$$\left\{m - \Delta[(\gamma\phi_x - \gamma^2 m\phi_{xy} + \ldots) + (\frac{1}{2}\gamma^2\phi_x{}^2 - \gamma^3 m\phi_x\phi_{xy} + \ldots)\right.$$

$$\left. + (\frac{1}{2}\gamma^2\phi_y{}^2 - \gamma^3 m\phi_y\phi_{yy} + \ldots)]\right\}\left\{\gamma\frac{dm}{dx} - [(\gamma^2\phi_{xx} - \gamma^3(m\phi_{xy})_x\right.$$

$$+ \ldots) + (\gamma^3\phi_x\phi_{xx} - \gamma^4(m\phi_x\phi_{xy})_x + \ldots) + (\gamma^3\phi_y\phi_{yx}$$

$$\left. - \gamma^4(m\phi_y\phi_{yy})_x + \ldots)]\right\}$$

$$= \frac{1-\Delta}{2} \cdot C_f \cdot [1 + (2\gamma\phi_x - 2\gamma^2 m\phi_{xy} + \ldots)$$

$$+ (\gamma^2\phi_x{}^2 - 2\gamma^3 m\phi_x\phi_{xy} + \ldots) + (\gamma^2\phi_y{}^2 - 2\gamma^3 m\phi_y\phi_{yy} + \ldots)]$$

$$0 < x < +\infty \quad y=0 \qquad \text{(III.25)}$$

$$m - \Delta[(\gamma\phi_x - \gamma^2 m\phi_{xy} + \ldots) + (\frac{1}{2}\gamma^2\phi_x{}^2 - \gamma^3 m\phi_x\phi_{xy} + \ldots)$$

$$+ (\frac{1}{2}\gamma^2\phi_y{}^2 - \gamma^3 m\phi_y\phi_{yy} + \ldots)] = 0$$

$$-\infty < x < 0 \quad y=0 \qquad \text{(III.26)}$$

$$\phi_y - m\gamma\phi_{yy} + \ldots = -(1 + \gamma\phi_x - m\gamma^2\phi_{xy} + \ldots)\frac{dm}{dx}$$

$$-\infty < x < +\infty \quad y=0 \qquad \text{(III.27)}$$

The resultant boundary value problem is shown in Figure III.6.

IV. SOLUTION OF BOUNDARY VALUE PROBLEM

A solution to the boundary value problem of Chapter III is sought in the form of an asymptotic expansion valid as the slenderness parameter γ and the density difference ratio Δ tend to zero. Only the latter is an arbitrary parameter, ranging from .01 to .15 for typical oils. The former is intrinsicly determined by the solution itself, and has been assumed small solely on the basis of experimental observation. The solution is written as follows:

$$m = M_{00} + \gamma M_{10} + \Delta M_{01} + \gamma^2 M_{20} + \gamma\Delta M_{11} + \Delta^2 M_{02} + \ldots$$

$$\phi = \phi_{00} + \gamma\phi_{10} + \Delta\phi_{01} + \gamma^2\phi_{20} + \gamma\Delta\phi_{11} + \Delta^2\phi_{02} + \ldots$$

Substituting these expressions in Equations (III.25), (III.26), and (III.27), and equating like coefficients, one obtains a set of problems which are linear in both the dynamic and kinematic boundary conditions, as well as the differential equation. Moreover, the dynamic condition becomes an explicit expression for the depth of the slick. When this depth is substituted into the kinematic condition, one obtains a simple boundary condition on the free surface and oil-water interface. Presented below are the solutions for the first five terms in

m, and problems for the first five terms in ϕ.

Solution for M_{00}; Problem for ϕ_{00}

The largest term on the left hand side of Equation (III.25) is of order γ. The largest term on the right hand side is $C_f/2$. It can be assumed, therefore, that γ is the same order of magnitude as C_f, and that one can express C_f as γC_f^*, where C_f^* is an order one quantity.

The dynamic boundary condition becomes:

$$M_{00} = 0 \qquad -\infty < x < 0$$

$$M_{00} \frac{d}{dx} M_{00} = \frac{1}{2} C_f^*(x) \qquad \text{(IV.1)}$$

$$M_{00} = \sqrt{\int_0^x C_f^*(x)\, dx} \qquad 0 < x < +\infty \qquad \text{(IV.2)}$$

Thus, the assumption of slenderness is equivalent to the assumption that dynamic terms are an order of magnitude smaller than those of viscosity and hydrostatics.

The kinematic condition becomes:

$$\phi_{00y} = -M_{00}' \qquad -\infty < x < +\infty \quad y=0 \qquad \text{(IV.3)}$$

where the prime denotes differentiation.

Solution for M_{10}; Problem for ϕ_{10}

So far the coefficient of friction has been based on local velocity. Due to the higher-order velocity terms, integrals of this friction coefficient will appear in all the higher order terms for slick depth. For simplicity, however, the friction coefficient will now be based on free stream speed. The right hand side of Equation (III.25) becomes merely $(1-\Delta)/2 \cdot C_f$.

The dynamic boundary condition becomes:

$$M_{10} = 0 \qquad -\infty < x < 0$$

$$\frac{d}{dx}\,(M_{00}M_{10}) = M_{00}\phi_{00xx} \tag{IV.4}$$

$$M_{00}M_{10} = \int_0^x M_{00}\phi_{00xx}\,dx$$

Integrating by parts:

$$M_{00}M_{10} = -\int_0^x \phi_{00x}M_{00}'\,dx + M_{00}\phi_{00x}$$

(IV.5)

$$M_{10} = -\frac{1}{M_{00}} \int_0^x \phi_{00x}M_{00}'\,dx + \phi_{00x} \qquad \begin{matrix} 0 < x < +\infty \\ y=0 \end{matrix}$$

Thus, the first order solution consists of two terms. The first represents the build-up of the slick due to dynamic pressure acting horizontally. The second term is the sucking down of the slick locally due to the local reduction in pressure.

The kinematic condition becomes:

$$\phi_{10y} = -M_{00}'\phi_{00x} + M_{00}\phi_{00yy} - M_{10}'$$

Using Laplace's equation, this becomes:

$$\phi_{10y} = -[M_{00}\phi_{00x} + M_{10}]' \qquad -\infty < x < +\infty \quad y=0 \tag{IV.6}$$

Solution for M_{01}; Problem for ϕ_{01}

Dynamic condition:

$$M_{01} = 0 \qquad -\infty < x < 0$$

$$\frac{d}{dx} M_{01}M_{00} = -\frac{1}{2} C_f^* \tag{IV.7}$$

$$M_{01} = -\frac{1}{2} M_{00} \int_0^x C_f^*(x)dx = -\frac{1}{2} \sqrt{\int C_f^*(x)dx} = -\frac{1}{2} M_{00} \qquad 0 < x < +\infty \tag{IV.8}$$

Kinematic condition:

$$\phi_{01y} = -M_{01}' \qquad -\infty < x < +\infty \tag{IV.9}$$

Solution for M_{20}; Problem for ϕ_{20}

Dynamic condition:

$$M_{20} = 0 \qquad -\infty < x < 0$$

$$\frac{d}{dx}(M_{00}M_{20}) - M_{10}\phi_{00xx} + \frac{d}{dx}\left(\frac{M_{10}^2}{2}\right) - M_{00}\phi_{10xx}$$

$$- M_{00}\phi_{00x}\phi_{00xx} - M_{00}\phi_{00y}\phi_{00yx} \tag{IV.10}$$

$$+ M_{00}(M_{00}\phi_{00xy})_x = 0$$

$$M_{20} = \frac{1}{M_{00}}\int_0^x M_{10}\phi_{00xx} + M_{00}\phi_{10xx} + M_{00}\phi_{00x}\phi_{00xx}$$

$$+ M_{00}\phi_{00y}\cdot{}_{00yx} - M_{00}(M_{00}\phi_{00xy})_x dx - \frac{M_{10}^2}{2M_{00}}$$

Integrating by parts, and using the zeroth order kinematic condition:

$$M_{20} = -\frac{1}{M_{00}} \int_0^x \phi_{00x} M_{10}' + \phi_{10x} M_{00}' + \frac{\phi_{00x}^2}{2} M_{00}'$$

$$- 2M_{00} M_{00}' M_{00}'' - M_{00}^2 M_{00}''' \, dx - \frac{M_{10}^2}{2M_{00}}$$

$$+ \frac{M_{10}\phi_{00x}}{M_{00}} + \phi_{10x} + \frac{\phi_{00x}^2}{2} \qquad \begin{matrix} 0 < x < +\infty \\ y=0 \end{matrix} \qquad \text{(IV.11)}$$

Once again, many of the terms in M_{20} are recognizable as "build-up" and "suck-down" forces. Others are not so obvious.

Kinematic condition:

$$\phi_{20y} = -\frac{M_{00}^2}{2} \phi_{00yyy} + M_{10}\phi_{00yy} + M_{00}\phi_{10yy}$$

$$- \phi_{00x} M_{10}' - \phi_{10x} M_{00}' + M_{00} M_{00}' \phi_{00xy} - M_{20}'$$

Applying Laplace's equation, and the zeroth order kinematic condition,

$$\phi_{20y} = -[M_{00}(\phi_{10x} + \frac{1}{2} M_{00}M_{00}") + M_{10}\phi_{00x} + M_{20}]'$$

$$-\infty < x < +\infty \quad y=0 \qquad \text{(IV.12)}$$

Solution for M_{11}; Problem for ϕ_{11}

Dynamic condition:

$$M_{11} = \phi_{00x} \qquad -\infty < x < 0, \ y=0$$

$$\frac{d}{dx}(M_{00}M_{11}) + \frac{d}{dx}(M_{10}M_{01}) - \frac{d}{dx} M_{00}\phi_{00x}$$

$$- M_{01}\phi_{00xx} - M_{00}\phi_{01xx} = 0 \qquad \text{(IV.13)}$$

$$M_{11} = \frac{1}{M_{00}} \int_0^x M_{00}'\phi_{00x} + M_{01}\phi_{00xx} + M_{00}\phi_{01xx} dx$$

$$- \frac{M_{10}M_{01}}{M_{00}}$$

Integrating by parts,

$$M_{11} = \frac{1}{M_{00}} \int_0^x M_{00}'\phi_{00x} - M_{01}'\phi_{00x} - M_{00}'\phi_{01x}dx$$

$$- \frac{M_{10}M_{01}}{M_{00}} + \frac{\phi_{00x}M_{01}}{M_{00}} + \phi_{01x} \qquad \begin{matrix} 0 < x < +\infty \\ y=0 \end{matrix} \qquad \text{(IV.14)}$$

Kinematic condition:

$$\phi_{11y} = M_{01}\phi_{00yy} + M_{00}\phi_{01yy} - \phi_{01x}M_{00}' - \phi_{00x}M_{01}' - M_{11}'$$

Using Laplace's equation,

$$\phi_{11y} = -[\phi_{00x}M_{01} + \phi_{01x}M_{00} + M_{11}]' \qquad \begin{matrix} -\infty < x < +\infty \\ y=0 \end{matrix} \qquad \text{(IV.15)}$$

Solution for M_{02}; Problem for ϕ_{02}

Dynamic condition:

$$M_{02} = 0 \qquad -\infty < x < 0 \qquad \text{(..V.16)}$$

$$\frac{d}{dx} M_{02}M_{00} + \frac{d}{dx} \frac{M_{01}^2}{2} = 0$$

$$M_{02} = -\frac{M_{01}^2}{2M_{00}} = -\frac{1}{8} M_{00} \qquad 0 < x < +\infty \qquad \text{(IV.17)}$$

Kinematic condition:

$$\phi_{02y} = -M_{02}' \qquad -\infty < x < +\infty \qquad \text{(IV.18)}$$

Solution for ϕ_{ij}

It can be seen that just as in the case of the thickness problem of thin airfoil theory (Van Dyke, 1964) the above linear problems all have the same form, to wit:

$$\nabla^2\phi_{ij} = 0 \qquad -\infty < x < +\infty,\ -\infty < y < 0$$

$$\nabla\phi_{ij} \to 0 \qquad x \to -\infty$$

$$\nabla\phi_{ij} \to 0 \qquad y \to -\infty$$

$$\phi_{ijy}(x,0-) = -F_{ij}(x)'$$

The solution to these problems can easily be obtained through the use of Green's theorem. If the slick is assumed to be symmetric, the solution can be analytically continued into the upper half plane, using the reflection principle due to Schwarz. If singularities are then distributed on the real axis, the dipole terms will cancel, and Green's theorem gives

an explicit expression for ϕ_{ij}:

$$\phi_{ij}(x,y) = \frac{1}{\pi} \int_{-\infty}^{\infty} \ell n \sqrt{(x - \xi)^2 + y^2}\, F_{ij}'(\xi) d\xi$$

For the solution to the higher order problem, one needs only $\phi_{ijx}(x,0-)$:

$$\phi_{ijx}(x,0-) = \frac{1}{\pi} \int_{-\infty}^{\infty} \frac{F_{ij}'(\xi)}{x - \xi}\, d\xi$$

The Singular Behavior at the Origin

The assumptions made in reducing the non-linear problem to a series of linear ones break down in the neighborhood of the leading edge, where a stagnation point must exist. The nature and extent of the non-uniformity of the solution will depend on the assumed behavior of the friction coefficient in this region. For the purposes of this investigation, it will be assumed that C_f can be expanded in a Taylor series about the origin.

The zeroth order solution for a constant value of friction coefficient is a parabola, $M_{00} = \sqrt{C_f x}$.* ϕ_{00x}, and

*Hereinafter, x and y will be measured in physical units and the star subscript on C_f will be dropped. The effect of this is to include γ dependence in M_{ij}, so that:

$$m = (M_{00}+M_{10}+M_{20}+\ldots)+(M_{01}+M_{11}+\ldots)\Delta + (M_{02}+\ldots)\Delta^2+\ldots$$

consequently M_{10}, are, somewhat surprisingly, zero everywhere on the positive real axis (Grobner and Hofreiter (1973) 211.10b). The kinematic condition on ϕ_{1y} is homogeneous, so that there is no first-order flow. M_{20} is easily calculated to be $C_f/4x$. The non-uniformity at the origin is due to the fact that the round-nosed slick is not slender near the leading edge.

It should be noted that a parabolic nose will result whenever the friction coefficient is non-zero at the leading edge. For a round-nosed slick where the friction coefficient can be expanded in the neighborhood of the origin in a Taylor series, $C_f = a + bx^2 + \ldots$ and $M_{00} = \sqrt{ax} + (b/4\sqrt{a})x^{3/2} + \ldots$ ϕ_{00x} and ϕ_{00xx} are finite, but non-zero, at the origin.* Equation (IV.5) shows that M_{10} is zero at the origin and by differentiating (IV.5) one can see that M_{10}' is finite there:

$$M_{10}' = \phi_{00xx} + \frac{M_{00}'}{M_{00}^2} \int_0^x M_{00}\phi_{00xx}\, dx$$

---

*By use of Liebnitz's rule, and integration by parts, it can be shown that:

$$\frac{d}{dx} \int_a^b \frac{m'(\xi)}{\xi - x}\, d\xi = \int_a^b \frac{m''(\xi)}{\xi - x}\, d\xi + \frac{m'(a)}{x-a} - \frac{m'(b)}{x-b}$$

If $M_{00}'(0) = 0$, ϕ_{00xx} will be finite at the origin if $M_{00}''(0) = 0$ or if $M_{00}'' \simeq 1/\sqrt{x}$ in the neighborhood of the origin.

From (IV.6) the kinematic condition on ϕ_{1y} goes as:

$$\phi_{1y} \simeq \frac{\text{const}}{\sqrt{x}} + \text{const} + \ldots$$

Although ϕ_{10x} is therefore singular as log x, M_{20} is singular as 1/x, as in the case with constant C_f.

In the derivation of expressions (IV.2), (IV.5), (IV.8), (IV.14), and (IV.17) it was assumed that the values of slick depth at the origin matched those on the free surface. Consequently, boundary terms from the integrations, such as $M_{00}M_{20}|_{x=0}$, were assumed to be zero, as were those resulting from integrations by parts. As a result, a non-integrable singularity in the integrand of (IV.11), for example, results in infinite values of M_{20} everywhere away from the origin. This is obviously less satisfactory than a singularity located at the origin, and since the dynamic boundary condition is singular at the origin, there is no reason that the value for M_{20} should match across the origin. Therefore, one can ignore the lower limit of integration where the integrand is singular, and the integrations by parts are valid.

If the friction coefficient is proportional to x in the neighborhood of the leading edge, the zeroth order solution is a wedge there, and ϕ_{00x} has a logarithmic singularity. $M_{10}(0)$

is non-zero, so that ϕ_{10x}, and consequently M_{20}, behave as $1/x$. The singularity encountered with this sharp-nosed zeroth order slick is due to the existence of a stagnation point in the zeroth order velocity field. One manifestation of this non-uniformity is that M_{10} goes to some non-zero value at the origin, while M_{00} goes to zero there. Consequently, there is a region of the slick where M_{10} is no longer small with respect to M_{00}.

If $C_f \simeq cx^2 + dx^3 + \ldots$ near the origin, $M_{00} \simeq \sqrt{c/3}\, x^{3/2} + \sqrt{3}/8\, d/\sqrt{c}\, x^{5/2}$. The zeroth order slick is cusped, and there is no stagnation point in the zeroth order flow. ϕ_{00x} is finite at the origin, so M_{10} goes to zero there. Furthermore, ϕ_{00xx} is finite, so that the first order slick is sharp-nosed, and ϕ_{10x} is only logarithmically singular. However, M_{20} is singular as $1/\sqrt{x}$ due to the fact that if M_{00} is cusped, and M_{10} is wedge-shaped, a region will exist where M_{10} is larger than M_{00}. Thus, it appears that it is not in general possible to circumvent the leading edge singularity by prescribing conditions on the behavior of C_f in that region.

The relationship between the assumed value of friction coefficient and the zeroth and first order slick depths in the neighborhood of the origin is shown in Figure IV.1.

The dynamic boundary conditions which determine M_{ij} are

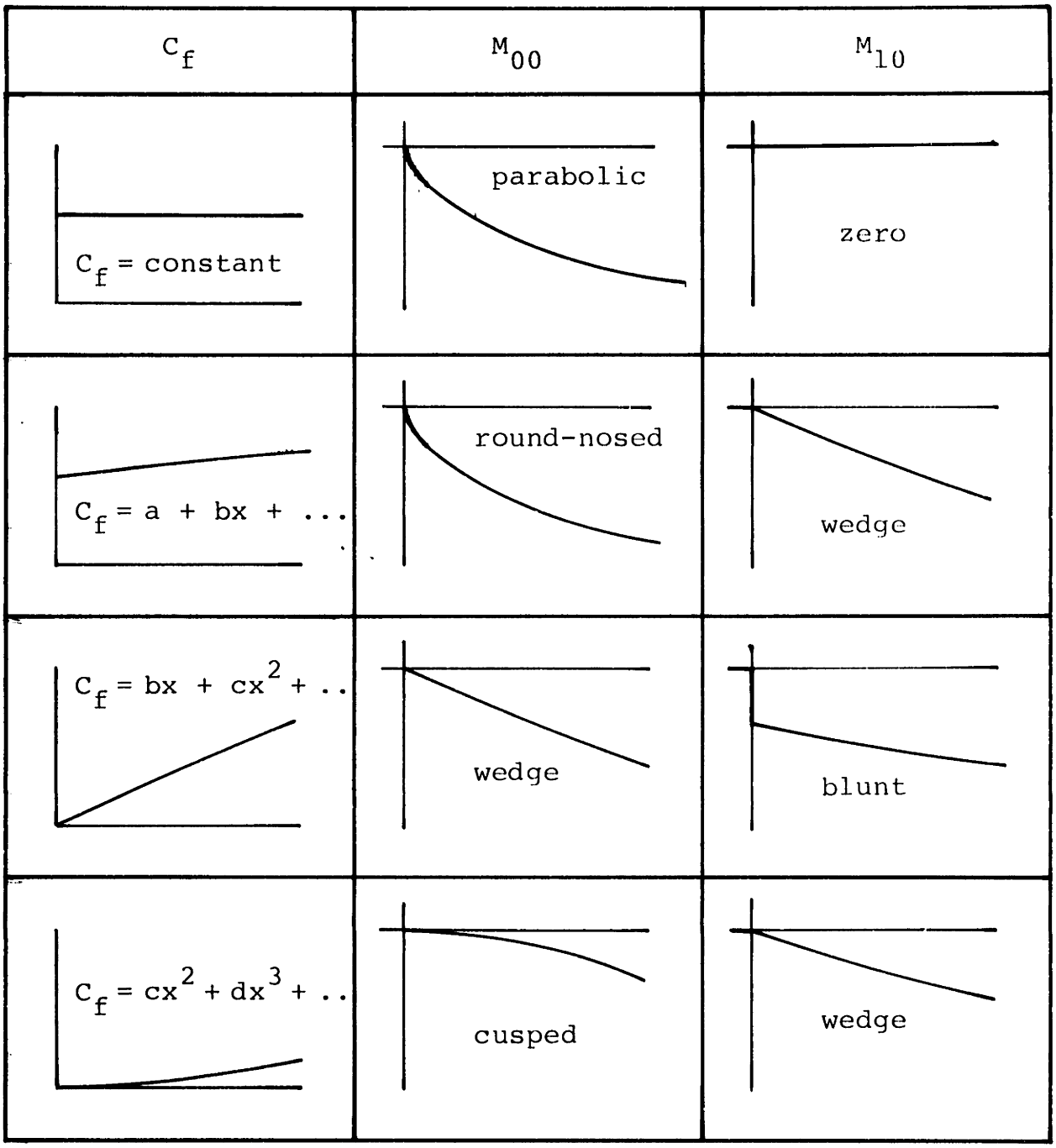

Figure IV.1 Relation Between C_f, M_{00} and M_{10} Near Origin

all of the form:

$$\frac{d}{dx}\,(M_{00}M_{ij}) = f(x)$$

It can be seen that eigensolutions exist for M_{ij}, namely:

$$M_{eig} = \frac{\text{Constant}}{M_{00}}$$

These solutions might be added to those depths which become singular at the leading edge, although Van Dyke's principle of minimum singularity would indicate that this can only be done when the strength of the singularity in the previously computed depth is as great or greater than that exhibited by M_{eig}. For example, in the case of the round-nosed slick, it was found that M_{20} was singular like $1/x$, whereas for that slick M_{eig} is singular as $1/\sqrt{x}$, so that M_{eig} could be added to M_{20} without increasing the degree of non-uniformity. The correct value for the constant in M_{eig} can only be determined by matching with an inner expansion valid in the region of non-uniformity. Of course the usual eigensolutions encountered in thin wing theory -- sources, dipoles, etc. located at the leading edge -- must be considered in the solution for ϕ_{ij} once M_{ij} is known.

Solutions for Various Friction Coefficients

There is very limited published data on the value of the interfacial friction coefficient. From measured slick set-up rates, Hoult found that far from the leading edge the friction coefficient was a constant, .0081 for soya oil, 30% less for fuel oil. Hale in the same way found values of .005 for diesel #2, and .011 for SAE 30. The values found in the headwave region, however, were much lower. These were obtained from extrapolating water velocity profiles to the interface, which appears to be a very unreliable method. It is significant that the interfacial velocities obtained the same way were much higher than one would expect.

In an experiment conducted by the author, the interfacial friction was measured by timing the relative speed of dye marks on the interface and the free surface, originally at the same horizontal position. The relationship between friction coefficient and this Δu is:

$$C_\rho = \frac{4}{\rho_w U^2} \cdot \frac{\mu}{t} \Delta u$$

The friction coefficient obtained for a 150cp oil at .55 fps was as shown in Figure IV.2, along with the depth of the slick and the relationship $C_f = (2\log Re - .65)^{-2.3}$, which derives from the logarithmic velocity distribution for turbulent flow

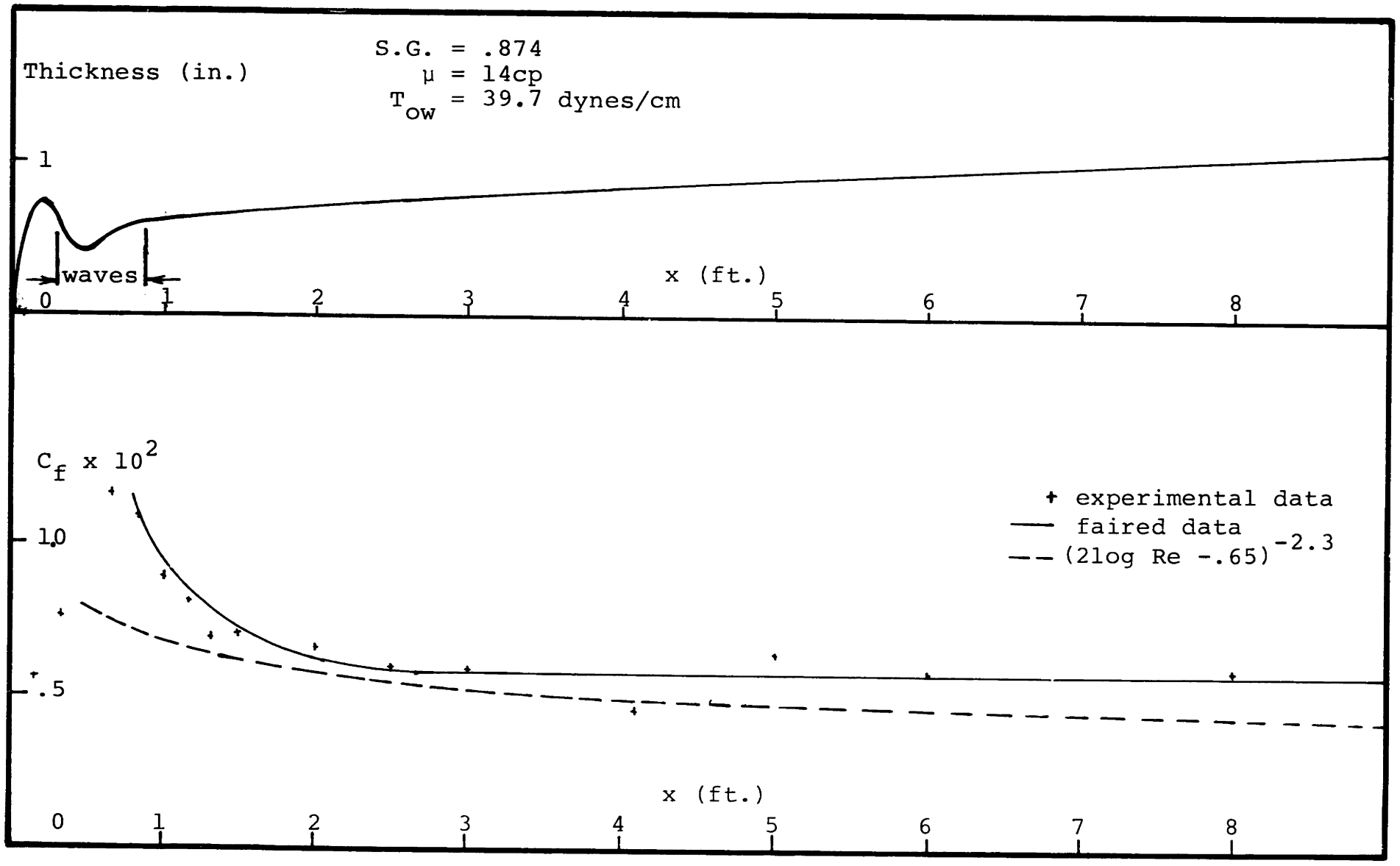

Figure IV.2 Oil Thickness and Interfacial Friction as Measured for Light Mineral Oil in .55 fps Current

over a flat, smooth, rigid plate (Schlichting, 1968). Data in the headwave region is not considered reliable, since diffusion of the dye was quite strong here. Furthermore, the dye velocities immediately behind the headwave may have been augmented by the mass transport of interfacial waves. The data behind this region, however, should be quite reliable. Here the friction appears to be approximately constant, and somewhat larger than that on a smooth, flat plate. From Schlichting, a constant value of $C_f = .0057$ corresponds to a constant relative roughness of $x/k_s = 2 \times 10^3$, although the Reynolds numbers here are significantly smaller than those at which a flat plate with this relative roughness is in the completely rough regime.

Some idea of the magnitude of the friction forces in the headwave region can be gained from the zeroth order solution to the slick thickness. This is:

$$M_{00} = \sqrt{\int C_f(x)dx}$$

In Figure I.2 is sketched a conceivable zeroth order monotonically increasing solution which might give rise to a solution resembling the observed geometry. M_{00} would therefore be .7 at x=4. To build up this much oil, C_f would have to be 0(.1) in this region.

Figure IV.3 shows the solution for M_{00} and M_{20} for $C_f=1$, along with the eigensolution for M_{20}. As previously noted, M_{10} is zero everywhere. M_{11} is zero for $x > 0$ but becomes infinite as $1/\sqrt{x}$ as $x \to 0$ along the negative real axis. The resultant solution ($M_{00} + M_{20}$) does not exhibit a headwave.

Outside the stagnation region, the friction coefficient can be expected to decrease as x increases. The M_{00} and M_{10} solutions for $C_f = .2/(1+x/4)$ are shown in Figure IV.4. Once again, no headwave is apparent.

Since C_f is here based on free stream velocity, it may increase with x in the stagnation zone. The solution for $C_f = .2x/(x+1)$ is shown in Figure IV.5. A very slight "headwave" exists in the solution to M_{10} very close to the leading edge, but it occurs in a region where the series appears non-convergent. By varying the constant in the denominator of C_f, the headwave can be shifted to a region where $M_{00} >> M_{10}$, but then the assumed stagnation zone is the entire headwave region. In either case, this headwave tendency is extremely weak.

As a final example, the solution for $C_f = .2x/(1+x/4)(x+1)$ is shown in Figure IV.6. This corresponds to a short stagnation zone, and a large scale decrease in friction with Reynolds number.

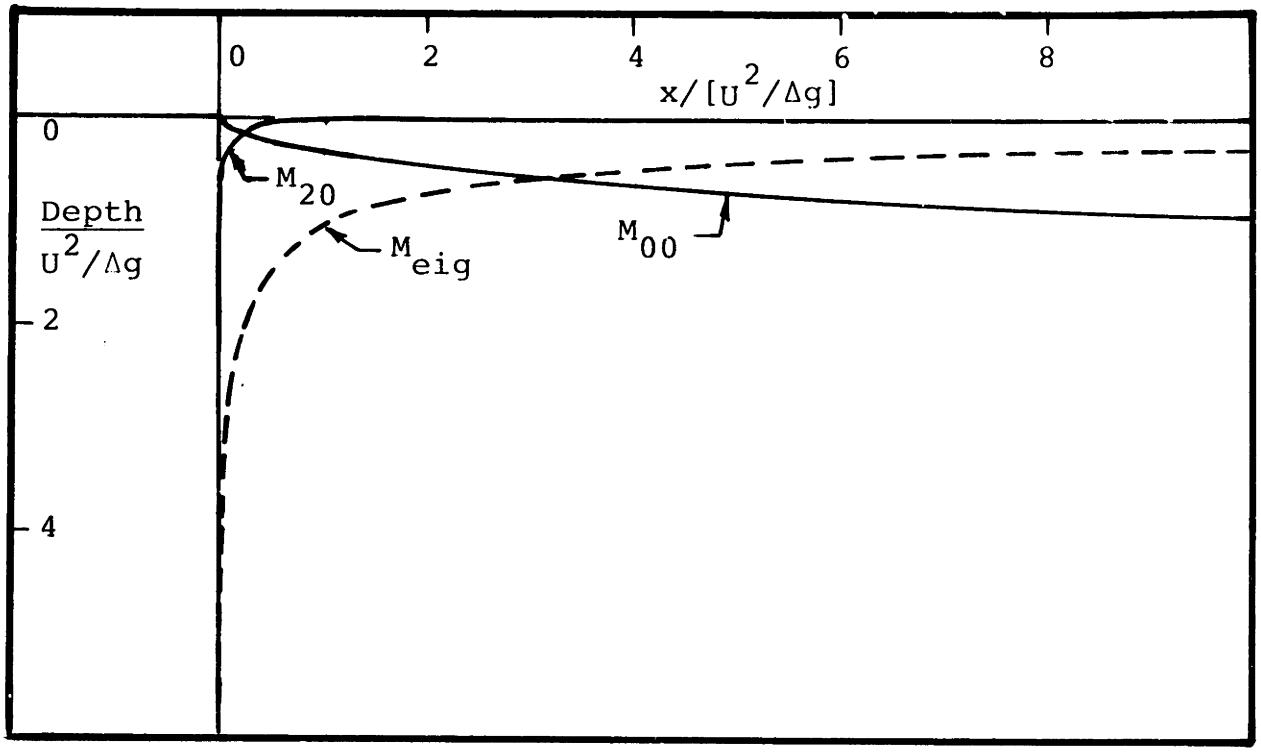

Figure IV.3 Solution for $C_f = .1$

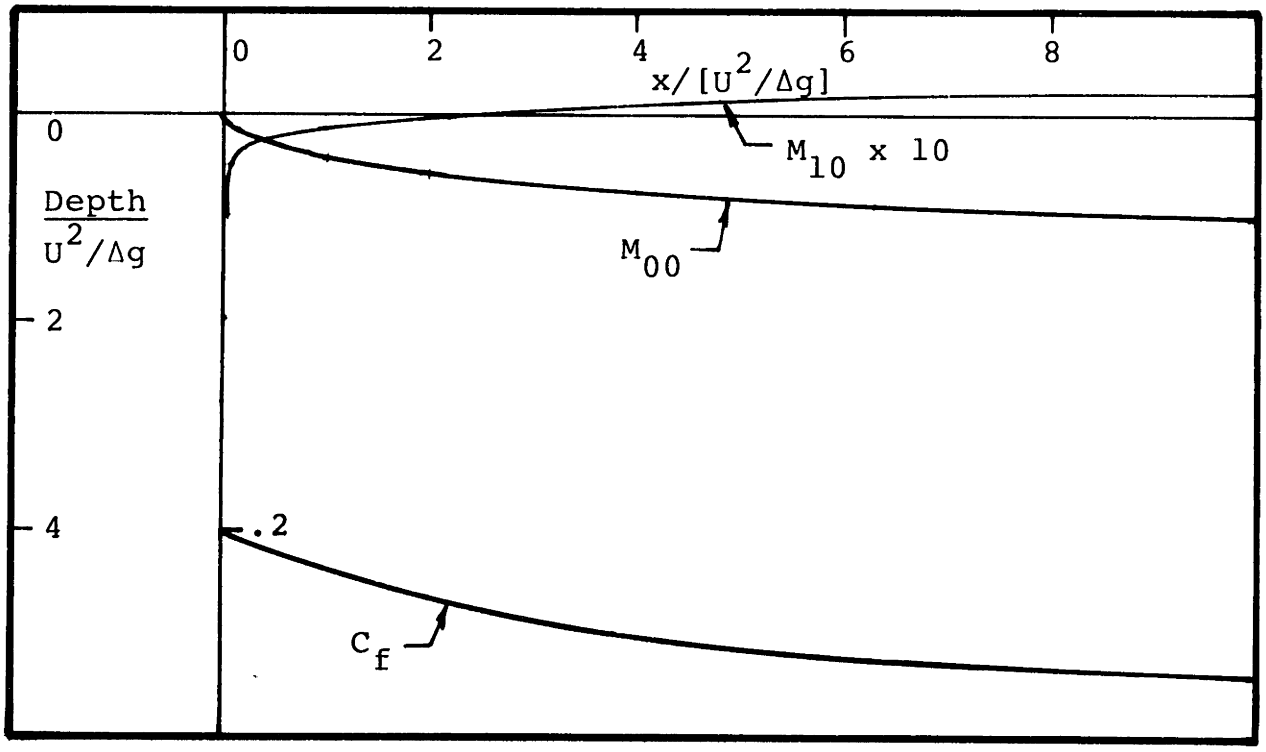

Figure IV.4 Solution for $C_f = .2/(1 + \frac{x}{4})$

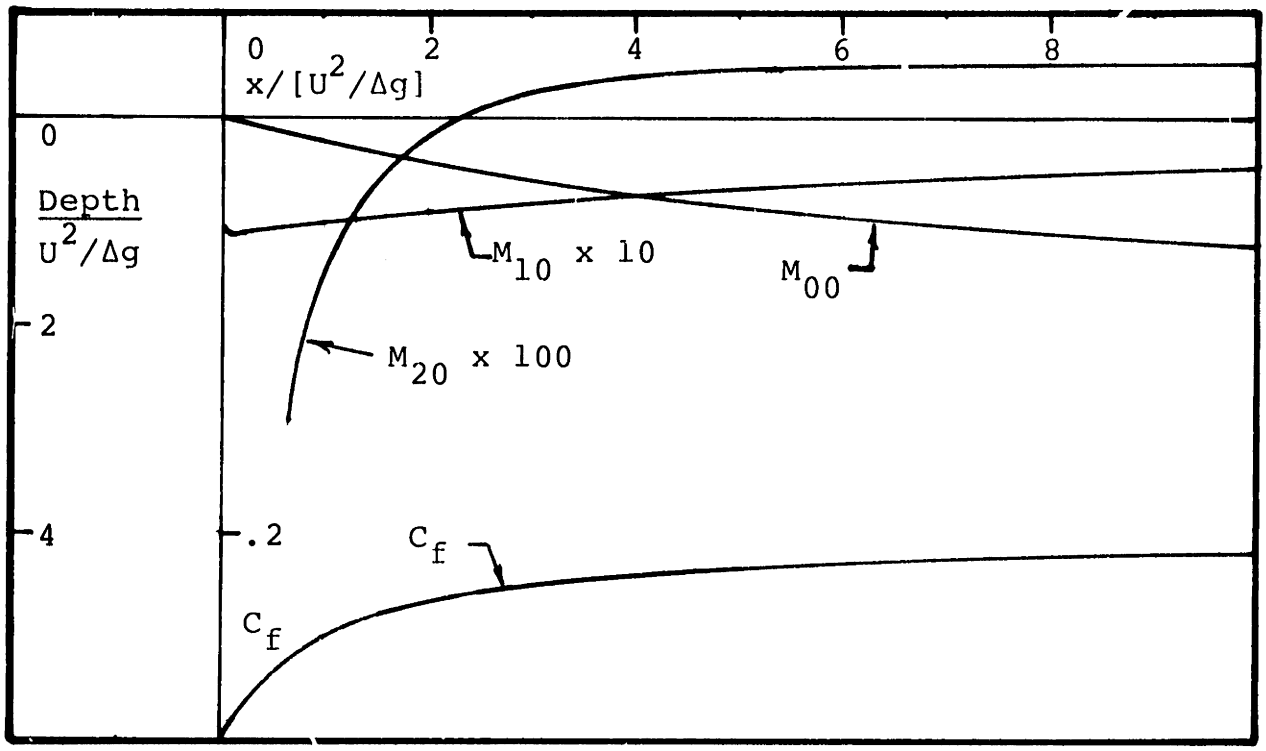

Figure IV.5 Solution for $C_f = .2x/(x+1)$

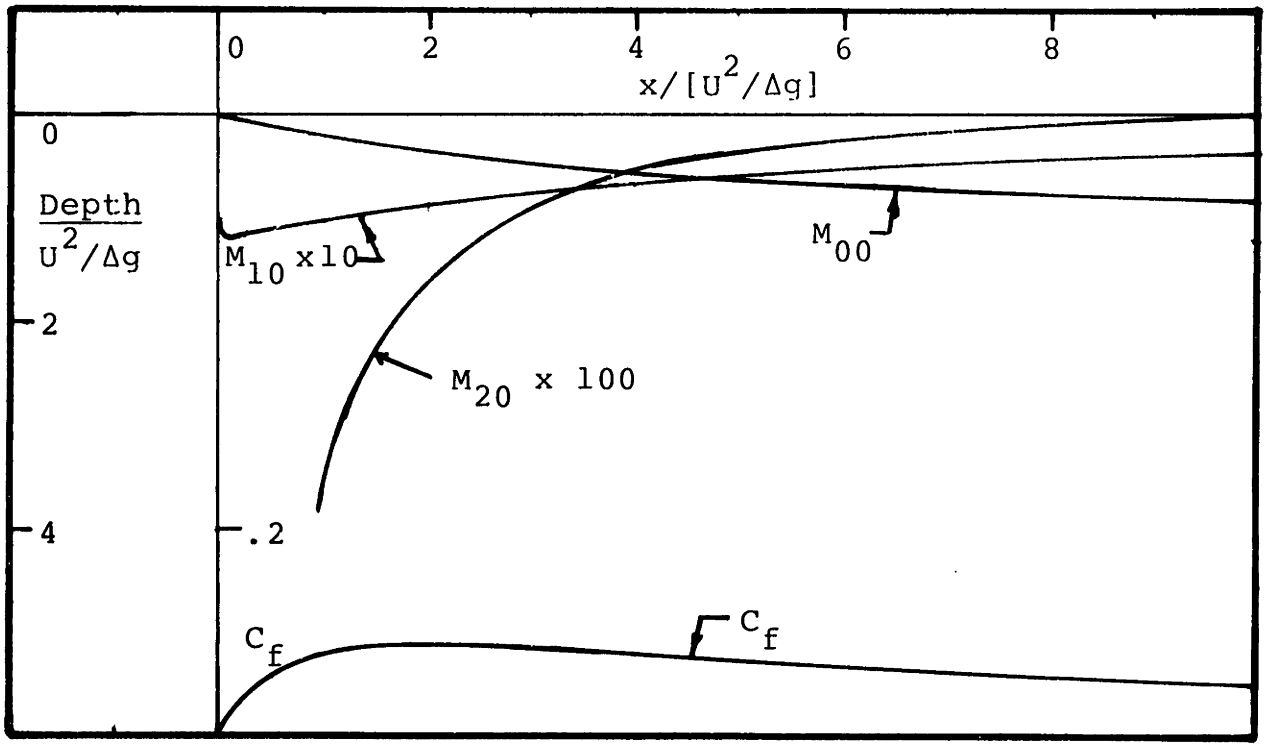

Figure IV.6 Solution for $C_f = .2x/[(1+\frac{x}{4})(x+1)]$

V. LEADING EDGE GEOMETRY

It was mentioned in Chapter II that von Kármán's model of a gravity current contained a 60° leading edge angle. This was due to the assumed balance between hydrostatic and dynamic forces. In the neighborhood of the stagnation point, the velocity squared must increase linearly, and the only corner flow where this occurs is one of 120° included angle. Although the present model includes friction, the 120° angle is still a possible configuration, since on the free surface side of the stagnation point, velocity squared must vary as x^n where $n \geq 1$. For a monotonically growing slick, $n \leq 2$. Possible configurations are shown in Figure V.1. In the case where the included angle is 120°, the values of relative density ratio and the local friction coefficient (based now on actual velocity) determines the orientation. In Appendix 4, the following relationship is found:

$$\phi_{LE} = \frac{2}{3} \sin^{1/2}(-\frac{2}{3}\beta + \frac{\pi}{3}) e^{i\beta} z^{3/2} \qquad (V.1)$$

where β is the solution to the following equation:

$$[-\frac{3}{2}\Delta - \frac{\sqrt{3}}{2} C_f(1-\Delta)]\cos^2(\frac{2}{3}\beta) + [-\sqrt{3} - \frac{\sqrt{3}}{2}\Delta + \frac{C_f(1-\Delta)}{2}]$$

$$\cdot \cos(\frac{2}{3}\beta)\sin(\frac{2}{3}\beta) + \frac{3}{2}(\Delta + \frac{1}{2}) = 0$$

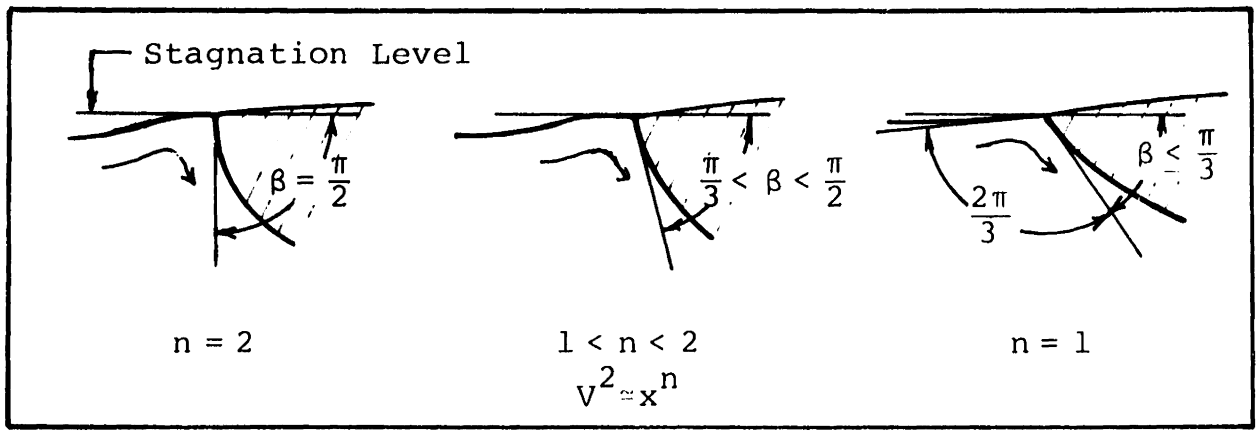

Figure V.1 Possible Flows in Neighborhood of Stagnation Point in Absence of Surface Tension

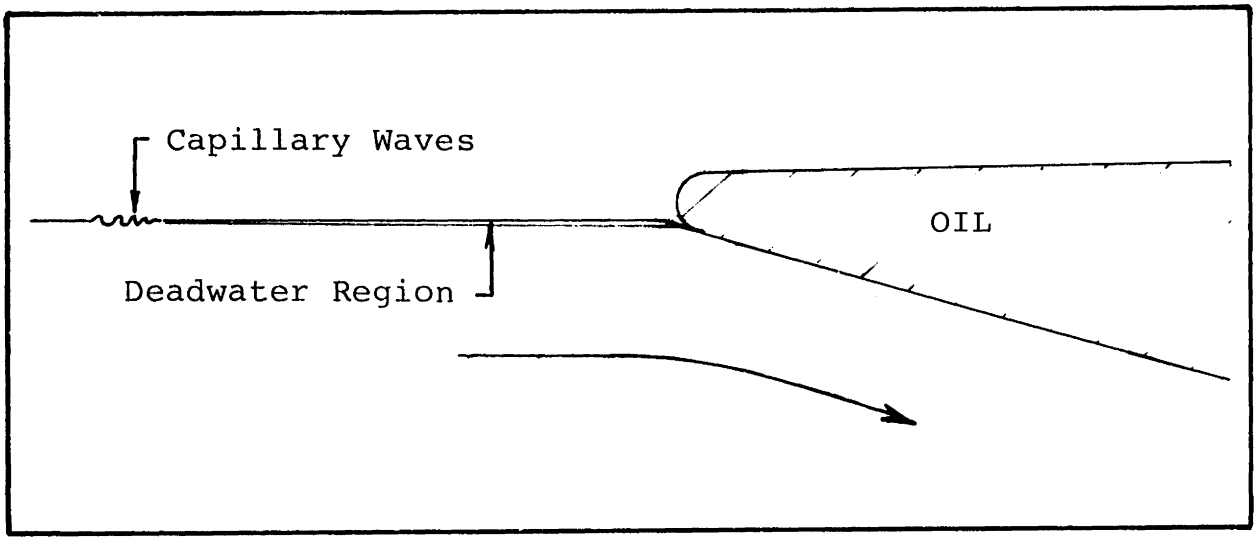

Figure V.2 Observed Leading Edge Flow

Here lengths are measured in units of $U^2/2g$. The shear stress has been assumed to vary linearly with distance from the leading edge. This would not be correct if the boundary layer structure is the same as for a rigid wall. The Falkner-Scan solution for flow around a rigid wedge is:

$$\tau \sim x^{[3\alpha/2(\pi-\alpha)] - 1/2}$$

where α is the wedge half-angle (Schlichting, 1968). For $\alpha = \pi/3$, the Falkner-Scan solution is $\tau \sim x^{1/4}$, and one would expect friction to dominate hydrostatic and dynamic forces at the stagnation point. If one insists that $\tau \sim x$, the required flow is one inside a right angle. But when the wedge angle becomes $\pi/2$, the hydrostatic forces no longer vary as x.

The flow configurations shown in Figure V.1 can only be expected to be valid in a region about the stagnation point of order $U^2/2g$ since this is the extent of the free surface rise. It is of order Δ times the magnitude of the oil slick's dimensions in the headwave region. Of the first five terms of the slick thickness expansion, only M_{11} includes any free surface rise at all. Therefore, it might be most fruitful to find the zero-Δ leading edge behavior, assuming that any modification due to non-zero Δ will be limited to an even smaller region. This simplification allows corner flow

solutions with included angles larger than 120°. These solutions, however, result in dynamic forces as well as shear stresses (as predicted by Falkner-Scan) which overwhelm the hydrostatic terms at the stagnation point.

To this point, only frictional, dynamic and hydrostatic forces have been considered in the leading edge region. Experimental observations indicate that other forces -- those associated with surface tension -- are important in the immediate region of the leading edge, and result in a force balance. The observed flow is shown in Figure V.2. It should be noticed that instead of rising to a stagnation point on the front of the oil slick, the water level drops, and the pressure increase due to the bending of the streamlines is balanced by surface tension. There appears to be no stagnation point. Furthermore, surface tension causes the oil slick to be of non-zero thickness at the point where the flow is first tangent to it. This means that a non-zero (but also non-infinite) shear stress can be balanced without an infinite slope. And since there is no stagnation point in the oil, the velocity of the oil at the interface can be non-zero where the interface is first wetted, tending to eliminate the infinite stress predicted by the Falkner-Scan solution for $\alpha < 45°$. Thus, surface tension serves to strike a force balance in the leading edge region. Indeed, it was found experimentally that

when a rigid boundary is substituted for the free surface the character of the leading edge was radically altered, becoming much more blunt, with the round nose typical of gravity currents on rigid surfaces.

The configuration shown in Figure V.2 is the observed flow around an oil with a negative spreading coefficient. Most spilled oil contains surfactants which result in positive spreading coefficients, and the leading edge flows for these cases might be quite different. However, the leading edge angle for these oils is not very different than for non-spreading oil. The geometry shown in Figure V.2 was observed by Lindenmuth for #2 Diesel fuel.

It should be noted from Figure V.2 that a dead water region exists on the free surface in front of the oil slick, extending as much as a foot in front of the leading edge, a distance far greater than the depth of the oil slick. This phenomenon is not restricted to flows around oil, and is also observed in front of barriers with shallow draft. The region is extremely thin, on the order of a millimeter, and water just below it moves at nearly free stream speed. Capillary waves are present at the leading edge of this region, and floating contaminants are trapped in it. Slow vertical vortices are present within the region. The origin of this dead water region is not clear. Three possibilities are that

it is a) composed of boundary layer fluid from the sides of the flume, in which case it does not exist in the field, b) fluid forced forward from the stagnation region in a surface jet, and c) a monolayer in which surfactant density varies with position so as to balance the shear force due to the water flowing beneath it. In any case, boundary layer growth starts well in front of the actual oil slick, and one expects finite shear stress at the leading edge of the oil.

It is apparent that the solution in the neighborhood of the leading edge must include the effects of surface tension. On the oil-water interface, however, it appears that the major effect is merely that the slick starts at a non-zero depth. Although surface tension and non-hydrostatic pressures are important in the nose of the slick, the model developed should be quite good over the wetted region. (The addition to the model of surface tension forces on the oil-water interface is relatively simple. Surface tension on the oil-air interface, however, leads to coupled differential equations for the depth and thickness of the oil layer in terms of water velocity.)

On the free surface in front of the oil slick surface tension must be included in the model. The dynamic boundary condition is:

$$\Delta(u + \frac{u^2}{2} + \frac{v^2}{2}) + m = \frac{\Delta^2 Tg}{\rho U^4} \frac{m_{xx}}{\sqrt{1+m_x^2}}$$

or, expressing m in regular Froude units of U^2/g:

$$u + \frac{u^2}{2} + \frac{v^2}{2} + m = \frac{Tg}{\rho U^4} \frac{m_{xx}}{\sqrt{1+m_x^2}}$$

The small length scale over which surface tension acts can be seen from the size of the coefficient leading the curvature term:

$$\frac{Tg}{\rho U^4} \simeq .01$$

If the curvature is large, perturbation velocities will not be particularly small. This means that depths of order Δ (measured in densiometric units) will be non-zero here. The correct way to match this solution to that valid in the bulk of the oil slick is not known.

VI. DISCUSSION AND RECOMMENDATIONS

Because observed slicks are quite slender and exhibit a very small, if any, stagnation region, it was hoped that the "slender slick" approximation would be valid over the region of the slick where headwave phenomena are present. However, it was found that the solution based on this approximation exhibits a fairly strong stagnation region, due to a zeroth order solution which responds to a non-zero shear force at the leading edge with an infinite slope there. Due to this singularity, eigensolutions with unknown coefficients appear in the higher order solutions. An "inner" solution, valid in the vicinity of the leading edge, is needed to determine the value of these coefficients in the "outer" solution. It was seen in Chapter V that surface tension plays a key role in the leading edge region, and it is felt that any inner solution which is going to successfully describe the leading edge flow must incorporate this phenomenon.

It has been remarked that data on interfacial friction in the neighborhood of the headwave is largely lacking. This is a less serious setback for the present theory than might first appear to be the case, due to the fact that observed headwave phenomena exhibit Froude rather than Reynolds scaling. Knowledge of the details of the distribution of shear stress would therefore seem inessential in investigating headwave effects. Just

the same, some general knowledge of this distribution is essential. No reliable experimental method has been developed to date, although it is felt that the dye streak method described herein still holds promise. It seems likely that for some combination of oil and dye the problem of interfacial diffusion will be less severe than that encountered by the author. The friction obtained from the inverse problem (Appendix 3) is surprisingly small in the leading edge region, but it is not known how sensitive it is to errors in the recording of the oil slick configuration. Deviations from hydrostatic of the pressures in the oil phase may be partially responsible for this anomalous behavior, and may introduce errors into experimental data obtained from the dye-streak method. The very low friction on the lee side of the headwave as computed from the inverse problem is of course significant, and may indicate the existence of flow separation. However, even if the flow is separated, and the present theory therefore inadequate, the question remains as to why the flow separates. What is the pressure gradient which exists along a contained oil slick which causes the flow to separate? The present theory should provide this information.

Two assumptions made--the hydrostatic pressure distribution in the oil phase and the lack of flow separation--may prove unjustified. If so, a uniformly convergent solution based on the

present theory will provide the answer to an academic question -- what is the steady configuration of a two-dimensional, hydrostatic fluid in front of a barrier, in the absence of flow separation? If not -- that is, if the simplifications are justified, the solution will provide a realistic description of a contained oil spill, and will provide a basis for understanding the interfacial instabilities which presently hamper oil spill clean-up operations.

REFERENCES

Benjamin, T.B., 1968, "Gravity Currents and Related Phenomena," Journal of Fluid Mechanics, Vol. 31, p. 209.

Briggs, R.J., 1964, Electron-Stream Interaction with Plasmas, Cambridge, Massachusetts: M.I.T. Press.

Drazin, P.G., 1970, "Kelvin-Helmholtz Instability of Finite Amplitude," Journal of Fluid Mechanics, Vol. 42, p. 321.

Gröbner, W. and Hofreiter, N., 1973, Integraltafel zweiter teil Bestimmte Integrale, Wein: Springer-Verlag.

Hale, L.A., Norton, D.J., and Rodenberger, C.A., 1974, "The Effects of Currents and Waves on an Oil Slick Retained by a Barrier," U.S. Coast Guard Report No. CG-D-53-75.

Hoult, D.P., 1970, "Containment of Oil Spills by Physical and Air Barriers," M.I.T. Fluid Mechanics Laboratory Report.

Jones, W.T., 1972, "Instability at an Interface Between Oil and Flowing Water," Journal of Basic Engineering, Vol. 94, No. 4, p. 874.

Keulegan, G.H., 1958, "The Motion of Saline Fronts in Still Water," National Bureau of Standards Report 5831.

Lamb, H., 1932, Hydrodynamics, 6th edition, Cambridge University Press (Dover edition, 1945).

Leibovich, S., 1976, "Oil Slick Instability and the Entrainment Failure of Oil Containment Booms," Journal of Fluids Engineering, Vol. 98, No. 1, p. 98.

Lindenmuth, W.T., Miller, E.R., and Hsu, C.C., 1970, "Studies of Oil Retention Boom Hydrodynamics," Hydronautics, Inc. Report 7013-2.

Middleton, G.U., 1966, "Experiments on Density and Turbidity Currents: I. Motion of the Head," Canadian Journal of Earth Science, Vol. 3, p. 523.

Milgram, J.H., 1971, "Forces and Motions of a Flexible Floating Barrier," Journal of Hydronautics, Vol. 5, No. 2, p. 41.

Milgram, J.H., 1976, personal conversation.

Milgram, J.H. and Van Houten, R.J., 1974, "Hydrodynamics of the Containment of Oil Slicks," 10th ONR Symposium on Naval Hydrodynamics.

Miller, E.R., Lindenmuth, W.T., Lehr, W.E., and Abrahams, R.N., 1972, "Experimental Procedures Used in the Development of Oil Retention Boom Designs," Marine Technology, Vol. 9, No. 3, p. 317.

Prandtl, L., 1952, Essentials of Fluid Dynamics, New York: Hafner.

Prandtl, L. and Tietjens, O.G., 1934, Applied Hydro- and Aeromechanics, New York: McGraw-Hill (Dover edition, 1957).

Schlichting, H., 1968, Boundary Layer Theory, 6th edition, New York: McGraw-Hill.

Van Dyke, M., 1964, Perturbation Methods in Fluid Mechanics, New York: Academic Press.

von Kármán, T., 1940, "The Engineer Grapples with Non-Linear Problems," Bulletin of the American Mathematical Society, Vol. 46, p. 615.

Wicks, M., 1969, "Fluid Dynamics of Floating Oil Containment by Mechanical Barriers in the Presence of Water Currents," Proceedings of the Joint Conference on the Prevention and Control of Oil Spills (American Petroleum Institute and U.S. Federal Water Pollution Control Administration).

Wilkinson, D.L., 1972, "Dynamics of Contained Oil Slicks," Journal of the Hydraulics Division (ASCE), Vol. 98, No. 6, p. 1013.

Wilkinson, D.L., 1973, "Limitations to Length of Contained Oil Slicks," Journal of the Hydraulics Division (ASCE), Vol. 99, No. 5, p. 701.

Yih, C.-S., 1965, Dynamics of Nonhomogeneous Fluids, New York: Macmillan.

Zalosh, R.G., 1974, "A Numerical Model of Droplet Entrainment from a Contained Oil Slick," U.S. Coast Guard Report CG-D-65-75.

APPENDIX 1: FROUDE NUMBER EXPANSION

In the absence of experimental data, one might well assume that the relevant length scale of the contained oil slick problem is that over which the value of the friction coefficient changes significantly. With this scaling, the equilibrium equation becomes:

$$[\frac{m}{S} - \Delta(\frac{V^2-1}{2})][m_x - S\frac{d}{dx}(\frac{V^2-1}{2})] = (1-\Delta)V^2C_f(x)$$

where $S = U^3/\Delta g\nu$ is either the square of a Froude number based on frictional length or a Reynolds number based on Froude length. Although numerically large, it in fact may act as a small parameter, since away from the leading edge the frictional forces can be expected to change over a number of feet, rather than the diffusion length ν/U.

Tentatively, then, one might consider the following expansion of m and $(V^2-1)/2$:

$$m = \sqrt{S}(M_{00} + SM_{10} + \Delta M_{01} + S^2M_{20} + S\Delta M_{11} + \Delta^2M_{02})$$

$$B = \frac{V^2-1}{2} = \sqrt{S}(B_{00} + SB_{10} + \Delta B_{01} + S^2B_{20} + S\Delta B_{11} + \Delta^2B_{02})$$

The advantage of such an expansion is that the solution is valid for all values of Froude number as well as specific

gravity. This is unlike the expansion presented in Chapter IV, where the friction coefficient depends on Froude number [$C_f = C_f(S \cdot x)$].

Solutions for M_{00} and M_{10} are as follows:

$$M_{00} = \sqrt{\int_0^x C_f(x)\,dx}$$

$$M_{10} = \frac{1}{M_{00}} \int_0^x M_{00} \frac{d}{dx} B_{00}\, dx$$

$$= - \frac{1}{M_{00}} \int_0^x M_{00}' B_{00} dx + B_{00}$$

To first order in $\sqrt{S}$,

$$B_{00} = u_{00} = \frac{1}{\pi} \int_0^\infty \frac{M_{00}'}{x-\xi}\, d\xi$$

The first two terms in m are thus identical with those derived in Chapter IV. The neglected terms in B_{00} are of order $\sqrt{S}$ times the linear term, whereas the linear term in B_{10} is of order S times that of B_{00}. It is therefore not consistent to linearize B_{ij} after B_{00}. Instead, one must include terms such as u_{00}^2 and alter the series for m to include integer powers of S:

$$m = \sqrt{S}\ (M_{00} + SM_{10} + S^{3/2}M_{20} + \ldots)$$

If experimental data were lacking, this procedure would perhaps seem superior to one which scaled lengths with respect to Froude units. Both methods result in zeroth order problems which balance hydrostatic and frictional forces. It would appear that friction-based length scales should predominate. It is only after looking at experimental data that the importance of Froude scaling becomes obvious. In the light of this knowledge, it can be seen that the Froude-number expansion will have difficulty converging. Since the horizontal length scale increases with Froude number, M_{20} must essentially attempt to reproduce M_{10} further back from the leading edge. Higher order depths must similarly try to move the solution back. In order to converge the successive solutions M_{ij} must increase in magnitude less than geometrically. Certainly rapid convergence seems very unlikely.

APPENDIX 2: NUMERICAL SOLUTIONS

Milgram and Van Houten (1974) presented a numerical procedure for the solution of the constrained oil slick problem. They considered a finite slick, and performed a Glauert-type transformation [$x=\frac{1}{2}(1-\cos\theta)$] on the x-coordinate. The slick depth was represented by a Fourier expansion in the transformed coordinate. Dynamic pressure was linearized, and the resultant Cauchy integral analytically evaluated in terms of the Fourier coefficients. The equilibrium equation was then applied at a number of points along the slick, and the resultant non-linear system of equations solved by a Newton-Raphson scheme. The solution was found for successively higher Froude numbers. The initial guess for the first value of Froude number was taken to be the viscous-hydrostatic solution; that for higher Froude numbers the solution for the preceding Froude number.

This method of approach suffers from a number of weaknesses. Solving the equilibrium equation over a finite rather than semi-infinite slick can introduce boundary effects which are not present in the actual slick. The slick was assumed to be of constant depth behind the region where the equilibrium equation was satisfied. The effect of this constant depth region on the solution can only be ignored when the solution is found to approach a constant depth. This failing can be

rectified if, instead of a Glauert transformation, the transformation $\theta = \pi e^{-x}$ $(0 < x < \infty)$ is used. A Fourier expansion in θ is similar to an expansion in Laguerre polynomials in x in that they both have the same weighing function in the orthagonality relations. In this case the Cauchy integrals must be worked out numerically.

It was pointed out in Appendix 1 that scaling with respect to a frictional length scale is not appropriate for the present problem, and will result in a divergent Froude number expansion. The numerical procedure outlined by Milgram and Van Houten is in many ways equivalent to a Froude number expansion. At very low Froude numbers, the dynamic terms of the equilibrium equation are assumed to be small. The collocation procedure, moreover, will appear to confirm this assumption, since at low Froude numbers the headwave region of the slick will likely lie between the leading edge of the slick and the first collocation point. As Froude number is increased, the dynamic terms will be felt further back in the slick. The convergence problem of the Froude number expansion will be felt here in a tendency of the iteration scheme to converge to unrealistic solutions, or to fail to converge at all, unless very small steps in Froude number are taken. This fault is perhaps not intrinsic to the numerical scheme, however, since the same procedure could be used to solve a version of

the equilibrium equation wherein the relevant length scale was taken to be the densiometric Froude length. However, if this is done there is no obvious best choice for the initial guess.

The two most serious faults of this method are the linearization of pressure and the finite number of terms which can economically be used with a Newton-Raphson scheme. Due to the former limitation, the numerical solution is no more accurate than the expansion:

$$m = M_{00} + \gamma M_{10} + \Delta M_{01} + \Delta\gamma M_{11} + \Delta^2 M_{02} + \Delta^2\gamma M_{12}$$

$$+ \Delta^3 M_{03} + \ldots$$

where terms of order γ^2 and higher are ignored. Furthermore, this is the limit of accuracy, achieved if an infinite number of Fourier terms are taken. Considering the high cost of the iteration scheme and the limited accuracy obtainable, the numerical solution is seen to be quite inefficient.

It is, of course, possible to devise a numerical scheme which does not involve the linearization of pressures, or even the assumption of slenderness. The variables of the Newton-Raphson scheme can be taken to be the depth of the interface below the undisturbed free surface at various distances

behind the leading edge, and the singularity distribution located on the interface. The difficulty here is the determination of the influence coefficients, which in general will involve the solution of an integral equation. For an N-term description, every N influence coefficients will require the solution of an NxN matrix, so that each iteration will require N+2 solutions of an NxN matrix, instead of the one required by the linear scheme. Although some economies can no doubt be made, the procedure will still be expensive if a reasonable number of terms are taken, and should only be considered if the slenderness expansion proves non-convergent in the region of interest.

APPENDIX 3: THE INVERSE PROBLEM

The problem solved in Chapter IV was the determination of the slick geometry which results when a given distribution of shear stress is applied at the interface. This problem was complicated by the non-linearity of the equilibrium equation, and the slenderness of the slick had to be invoked in order to obtain an equivalent infinite set of linear equations.

The inverse problem is not so difficult. The problem consists of determining the interfacial shear stress which produces a given slick geometry. Since the equilibrium equation can be interpreted as an explicit expression for shear stress in terms of depth and velocity, the assumption of slenderness need not be made (except insofar as it is necessary for the assumption of hydrostatic pressures in the oil). Furthermore, the question of proper scaling is no longer so pressing as it is in the case of the direct problem.

Milgram (1976) solved this inverse problem. His approach was to measure slick depth in the flume at a known flow speed and with oil of known specific gravity. The free surface in front of the oil and the oil-water interface were modelled as a set of discrete line vortices, and the strength of these vortices found by solving the discrete form of the integral equation which equates normal velocity to zero along the boundary. Using the tangential velocities thus obtained, the

equilibrium equation yields the interfacial friction coefficient. Figure 3.1 shows the measured depth and computed friction for a .921 specific gravity oil at 1.0 fps flow speed.

The two significant results of this procedure are that a) there is very little friction on the front of the oil slick, and b) there is very little (sometimes negative) friction on the back of the headwave. The latter finding is somewhat condemning, since the theory assumes no separation, but the inaccuracies of measurement, and the anomalous result of low friction near the leading edge, where one expects large friction, make the results somewhat questionable.

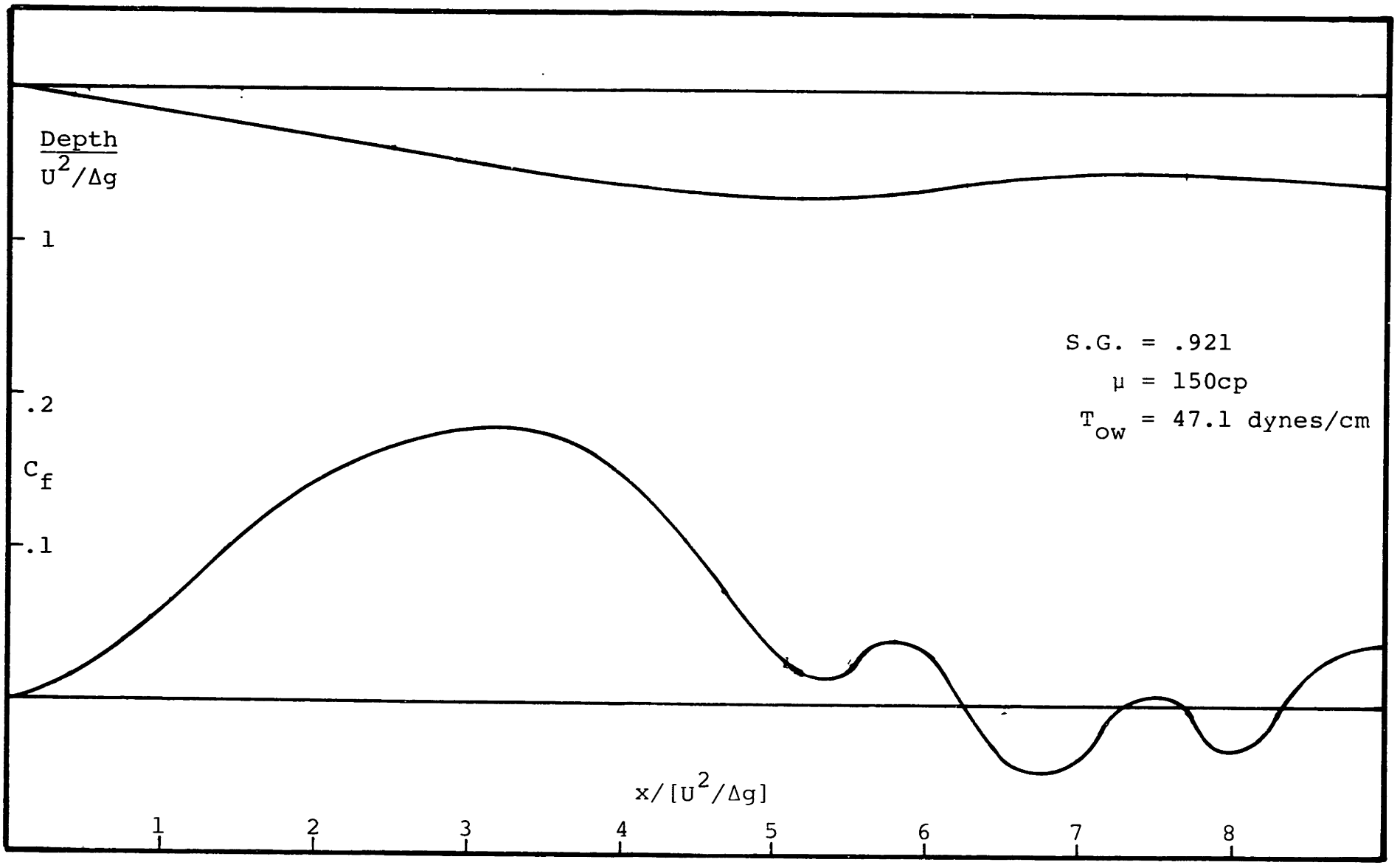

Figure 3.1 Interfacial Friction Computed from Inverse Problem for Heavy Mineral Oil in 1 fps Flow

APPENDIX 4: 120° INCLUDED ANGLE CORNER FLOW

Figure 4.1 shows the assumed configuration of the leading edge. The dynamic conditions on the two interfaces are:

$$D = V^2 \qquad \text{(water-air)} \qquad (4.1)$$

$$(D - V^2)(\Delta D_x - V_x^2) = (1-\Delta)V^2 C_f \qquad \text{(water-oil)} \qquad (4.2)$$

where all lengths are scaled in units of $U^2/2q$ and velocities in units of U. C_f is here based on local flow speed, and D is the depth of the interface below stagnation level.

Assume the flow is of the form:

$$\phi_{LE} = Az^n \qquad \text{where } A = |A|e^{i\beta} \text{ and } z = |z|e^{i\theta} = x + iy$$

$$\phi_{LE_z} = u - iv = nAz^{n-1} \qquad (4.3)$$

$$V^2 = |\phi_{LE_z}|^2 = |n^2A^2z^{2(n-1)}|$$

Applying the water-air boundary condition (4.1), and assuming that the water surface is not horizontal at the stagnation point, one obtains:

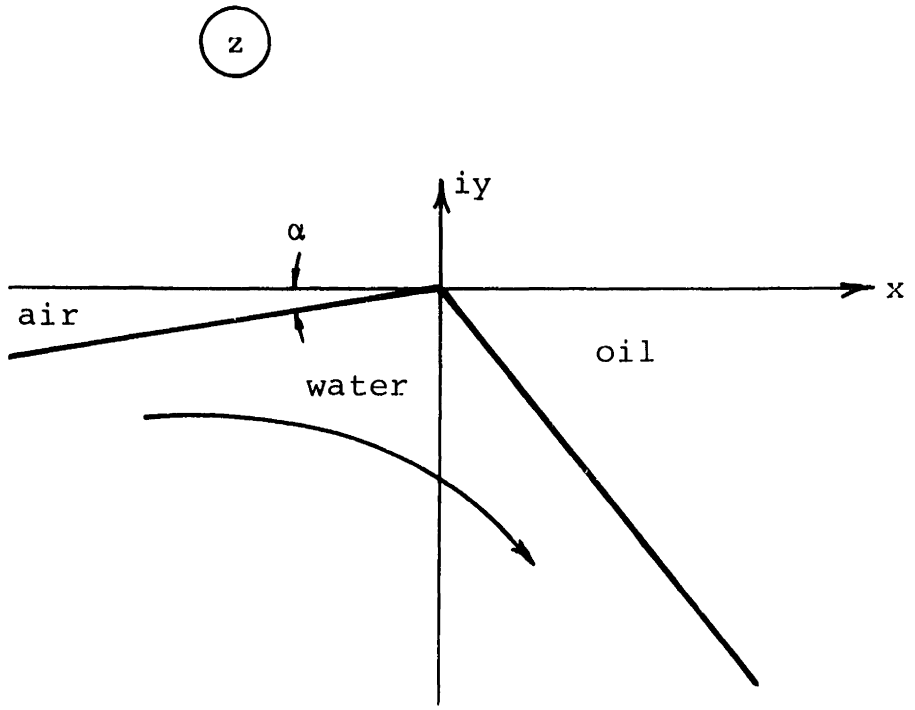

Figure 4.1 Corner Flow at Stagnation Point

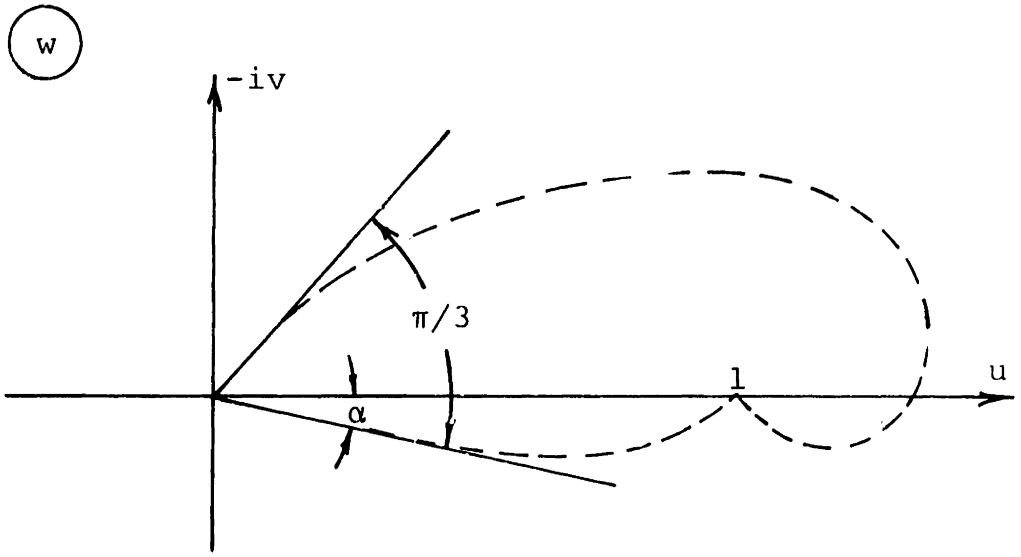

Figure 5.1 Hodograph Plane for Flow Around Oil Slick with 120° Corner Flow At Leading Edge

$$|z|\sin\alpha = |z^{2(n-1)}||A|^2 n^2$$

$$n = 3/2 \qquad |A| = \frac{2}{3}(\sin\alpha)^{1/2} \tag{4.4}$$

To find β, set $\text{Arg}(\phi) = \pi$ when $\theta = -(\pi-\alpha)$:

$$\beta - \frac{3}{2}(\pi-\alpha) = \pi \qquad \beta = \frac{5}{2}\pi - \frac{3}{2}\alpha = \frac{\pi}{2} - \frac{3}{2}\alpha \tag{4.5}$$

And to find the included angle, set $\text{Arg}(\phi) = 0$:

$$\beta + \frac{3}{2}\theta = 0 \qquad \theta = -\frac{2}{3}\beta = -\frac{\pi}{3} + \alpha$$

The included angle is $\frac{2\pi}{3}$. All flow characteristics are now known in terms of α, which is determined by the friction coefficient and relative density ratio.

On the oil-water interface,

$$D = |z|\sin(\frac{\pi}{3} - \alpha)$$

$$= |z|\sin(\frac{2}{3}\beta)$$

$$V^2 = |z|\sin\alpha = |z|\sin(-\frac{2}{3}\beta + \frac{\pi}{3})$$

$$\frac{d}{dx} = \frac{d}{d|z|}\frac{1}{\cos(2/3\beta)}$$

Substituting into Equation (4.2):

$$[\sin(\tfrac{2}{3}\beta) - \sin(-\tfrac{2}{3}\beta + \tfrac{\pi}{3})][\Delta\sin(\tfrac{2}{3}\beta) - \sin(-\tfrac{2}{3}\beta + \tfrac{\pi}{3})]$$

$$= C_f(1-\Delta)\sin(-\tfrac{2}{3}\beta + \tfrac{\pi}{3})\cos(\tfrac{2}{3}\beta)$$

Simplifying:

$$[\frac{3\sin(\frac{2}{3}\beta)}{2} - \frac{\sqrt{3}}{2}\cos(\tfrac{2}{3}\beta)][(\Delta+\tfrac{1}{2})\sin\tfrac{2}{3}\beta - \frac{\sqrt{3}}{2}\cos(\tfrac{2}{3}\beta)]$$

$$= C_f(1-\Delta)\cos(\tfrac{2}{3}\beta)[\frac{\sqrt{3}}{2}\cos(\tfrac{2}{3}\beta) - \frac{1}{2}\sin(\tfrac{2}{3}\beta)]$$

And further simplifying:

$$[-\tfrac{3}{2}\Delta - \frac{\sqrt{3}}{2}C_f(1-\Delta)]\cos^2(\tfrac{2}{3}\beta) + [-\sqrt{3} - \tfrac{\sqrt{3}}{2}\Delta + \frac{C_f(1-\Delta)}{2}]$$

$$\cdot \cos(\tfrac{2}{3}\beta)\sin(\tfrac{2}{3}\beta) + \tfrac{3}{2}(\Delta+\tfrac{1}{2}) = 0 \qquad (4.6)$$

Substituting (4.4) and (4.5) into (4.3), one gets:

$$\phi_{LE} = \frac{2}{3}\sin^{1/2}(-\tfrac{2}{3}\beta + \tfrac{\pi}{3})e^{i\beta z}z^{3/2}$$

where β is the solution to Equation (4.6).

APPENDIX 5: CONFORMAL MAPPING METHOD FOR ELIMINATION OF LEADING EDGE SINGULARITY

Figure 5.1 shows the possible leading edge configurations for a gravity current on a free surface in the absence of surface tension. The 120° included angle solution is the least blunt and perhaps for this reason the most likely. The local flow in the neighborhood of the 120° corner is given in Appendix 4. Certainly a series expansion based on slick slenderness cannot converge in the neighborhood of such a stagnation point. However, if the physical plane is first mapped with a conformal mapping function which satisfies certain conditions, the slick may be assumed slender about the real axis in the new plane. These conditions are:

1) $\zeta \simeq \phi_{LE}(z)$ as $z \to 0$
2) $\zeta \simeq z$ as $|z| \to \infty$
3) ζ is analytic in the lower half ζ-plane
4) ζ is sufficiently well behaved that the slick remains slender away from the leading edge.

Although the first three requirements can easily be met by any number of functions, the last one is quite restrictive. Since ϕ_{LE} contains a branch point at the origin, requirement (2) requires that another branch point be located at a finite

distance from the origin, and (3) dictates that it be located in the upper half of the ζ plane. The placement of this branch point will determine how well (4) is met.

Investigators of high Froude number free-streamline flows have found that they often know more about flow velocities than they do about flow boundaries. In these cases they resort to hodograph methods wherein they work with the $w = \phi_z$ plane rather than with the physical z plane. Although the present problem is one of low Froude number, and the simplifications of high Froude number flow are not appropriate, the hodograph technique is still useful in that some characteristics of the velocity field are known. The hodograph plane for the present problem is sketched in Figure 5.1.

Near the origin,

$$\phi \simeq A\, z^{3/2}$$

$$w = \phi_z \simeq \frac{3}{2} A\, z^{1/2}$$

or,

$$z \simeq \left(\frac{2}{3}\,\frac{1}{A}\right)^2 w^2$$

Letting $C = 2/(3A)$:

$$z \simeq C^2 w^2$$

Since at large distances the slick will appear to first order source-like (and possibly vortex-like) the proper correction to this leading edge solution is:

$$z = -\frac{C^2 w^2}{w-1} \tag{5.1}$$

as $|z| \to \infty$

$$w \simeq 1 - \frac{C^2}{z} = 1 + \frac{(Csc\alpha)e^{i3\alpha}}{z}$$

Because α is generally small, the perturbation velocity is largely that due to a source. The location of the branch point in the w plane can be found from Equation (5.1):

$$w^2 + \frac{z}{C^2} w - \frac{1}{C^2} z = 0$$

$$w = -\frac{z}{2C^2} + \sqrt{\frac{z^2}{4C^4} + \frac{z}{C^2}}$$

$$= \frac{-z + z^{1/2}(z + 4C^2)^{1/2}}{2C^2}$$

The second branch point is at:

$$z_{bp} = -4C^2 = 4\csc\alpha e^{i3\alpha}$$

Since α is generally small, $z_{bp} = (4/\alpha) + i12$. Thus, the branch point is not in the flow domain.

To obtain the mapping function itself, one needs only to integrate Equation (5.2). The result is:

$$\zeta = -\frac{z^2}{4C^2} + (\frac{z}{2C^2} + 1)\frac{z}{2}\sqrt{1 + (4C^2/z)}$$

$$- C^2 \ell n[(\frac{z}{2C^2} + 1) + \frac{z}{2C^2}\sqrt{1 + (4C^2/z)}] \qquad (5.3)$$

In order to find the profile in the z plane which corresponds to the real ζ axis, an iterative scheme such as Newton's method must be used. When this is done, it is found that the profile is not particularly slender. When the depths, slopes, and tangential velocities of this profile are substituted in Equation (4.2), one finds that well away from the leading edge the friction coefficient is quite large -- generally larger than .5 even when the leading edge angle corresponds to a much lower value.

So far the only correction made to the leading edge flow

has been that necessary to satisfy the condition at $|z| \to \infty$. Other singularities can be introduced as long as they do not affect the flow at the origin or at infinity. The simplest is another pole in the hodograph plane:

$$z = \frac{-aw^2}{(w-1)(w + a/C^2)} \tag{5.4}$$

where a is arbitrary and $w=-a/C^2$ is the location of the pole. Clearly the argument of a must lie in the range:

$$\frac{\pi}{3} - 4\alpha < arg\, a < 2\pi - 4\alpha$$

and one would expect the smoothest profile to correspond to a value approximately mid-way in this range.

Inverting this expression as before, one gets:

$$w = \frac{(1-\frac{a}{C^2})z + \sqrt{(\frac{a}{C^2} + 1)^2 z^2 + \frac{4a^2}{C^2} z}}{2(z+a)} \tag{5.5}$$

where the branch point is seen to be located at:

$$z_{bp} = \frac{-\frac{4a^2}{C^2}}{\frac{a^2}{C^4} + \frac{2a}{C^2} + 1}$$

For large values of $|\frac{a}{C^2}|$, $z_{bp} \to -4C^2$ as before, but for small

values, $z_{bp} \to -4C^2(a/C^2)^2$ so that the flow can be "turned around" much closer to the origin, hopefully resulting in a slender slick a short distance from the leading edge.

Integrating Equation (5.5), one gets:

$$\zeta = \frac{1-\frac{a}{C^2}}{2}\,[z - a\ell n(a+z)] + \frac{a+C^2}{2C^2}\left\{\sqrt{z^2 + \frac{4z}{(\frac{1}{C}+\frac{C}{a})^2}}\right.$$

$$+ \left[\frac{2}{(\frac{1}{C}+\frac{C}{a})^2} - a\right]\ell n\left[z + \frac{2}{(\frac{1}{C}+\frac{C}{a})^2} + \sqrt{z^2 + \frac{4z}{(\frac{1}{C}+\frac{C}{a})^2}}\right]$$

$$+ \sqrt{a^2 - \frac{4a}{(\frac{1}{C}+\frac{C}{a})^2}}\;\ell n$$

$$\left[\frac{\frac{2}{(\frac{1}{C}+\frac{C}{a})^2} - a}{\sqrt{a^2 - \frac{4a}{(\frac{1}{C}+\frac{C}{a})^2}}}\,z - \frac{2a}{(\frac{1}{C}+\frac{C}{a})^2}\Big/\sqrt{a^2 - \frac{4a}{(\frac{1}{C}+\frac{C}{a})^2}} - \sqrt{z^2 + \frac{4z}{(\frac{1}{C}+\frac{C}{a})^2}}\right.$$

$$\left.\vphantom{\frac{1}{1}}\right] \qquad z + a \qquad \left.\vphantom{\frac{1}{1}}\right]$$

(5.6)

Using Equation (5.6), the mapping of the real ζ axis onto the z plane produces more satisfactory results than when Equation (5.3) is used as the mapping function. For most values of $C_f(0)$, small values of $|a|$ (corresponding to a branch point close to the origin) yield rather large negative values of friction coefficient immediately behind the leading edge. Larger values of $|a|$ reduce this negative friction, or eliminate it, but at the expense of having a large positive value of friction coefficient ($\simeq .4$) further back in the slick, in the headwave region. Since C_f is based on local velocity, large values of $C_f(0)$ are probably most appropriate. (The Falkner-Scan solution for a rigid wedge predicts that the friction coefficient based on local velocity blows up as $x^{-3/4}$.) The solution for $\Delta=.1$, $C_f(0) = 10$, $a = 10e^{i4\pi/3}$ is shown in Figure 5.2.

A slender slick expansion in the ζ plane may have difficulty negating the rather large value of friction which results from this mapping. Certainly much care is necessary in assigning relative orders of magnitude to quantities resulting from the mapping procedure and those resulting from the slenderness expansion. Furthermore, the procedure must be repeated for each value of Δ, since the mapped quantities are in Froude units whereas the slenderness expansion is in densiometric Froude units. This approach has not been fully

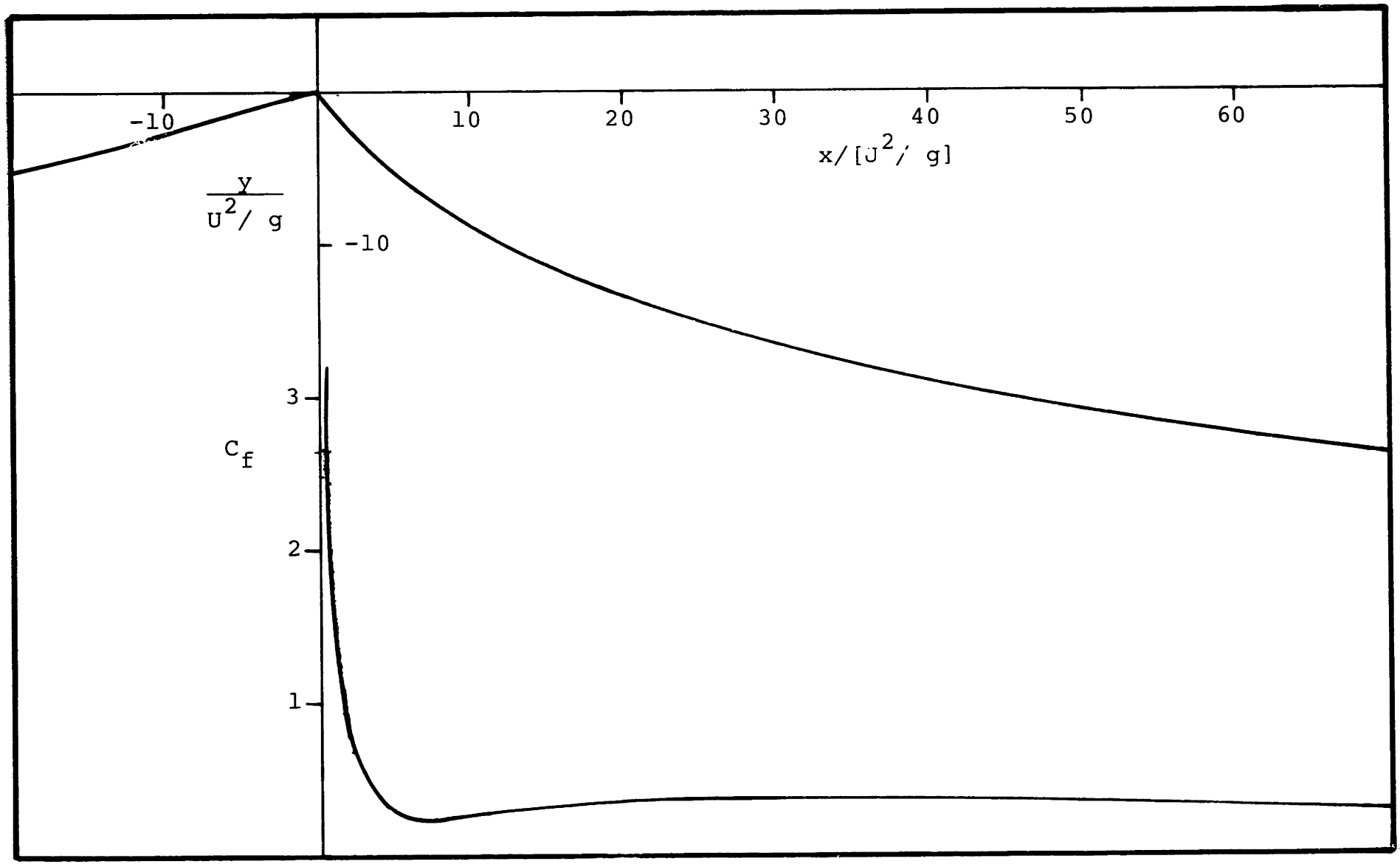

Figure 5.2 Mapping (Eq. 5.6) of Real ζ Axis onto z Plane, and Associated C_f for $\Delta = .1$, $C_f(0) = 10.$, $a = 10e^{i4\pi/3}$

evaluated, but in view of the observed effects of surface tension in the leading edge region, one must question the practical value of a pure viscous-hydrostatic-dynamic solution which produces leading edge angles five times as large as those observed.

APPENDIX 6: EXPERIMENTAL EQUIPMENT AND PROCEDURES

EQUIPMENT

Flume

All experiments were carried out in the Precision Flume, located in the Ocean Engineering Hydrodynamics Laboratory at M.I.T. A sketch of this flume is shown in Figure 6.1. The test section of this flume measures 18 inches wide by 24 inches deep by 20 feet long, and is constructed to a tolerance of 0.030 inches. The test section has glass sides and a glass bottom, allowing unobstructed observation. By varying the position of the downstream weir, and by controlling the speed of the propeller, water height in the test section and flow speed can be independently adjusted. The flow uniformity outside the boundary layers is within 5%, and free-stream turbulence is on the order of one percent of free stream speed.

Calibration

A 120-tooth gear is positioned on the propeller shaft opposite a magnetic pick-up, giving approximately 500 to 650 pulses per second. These pulses are counted by a HP-522B electronic counter. By timing floating chips, flow speeds (at the surface) were calibrated against counter output and

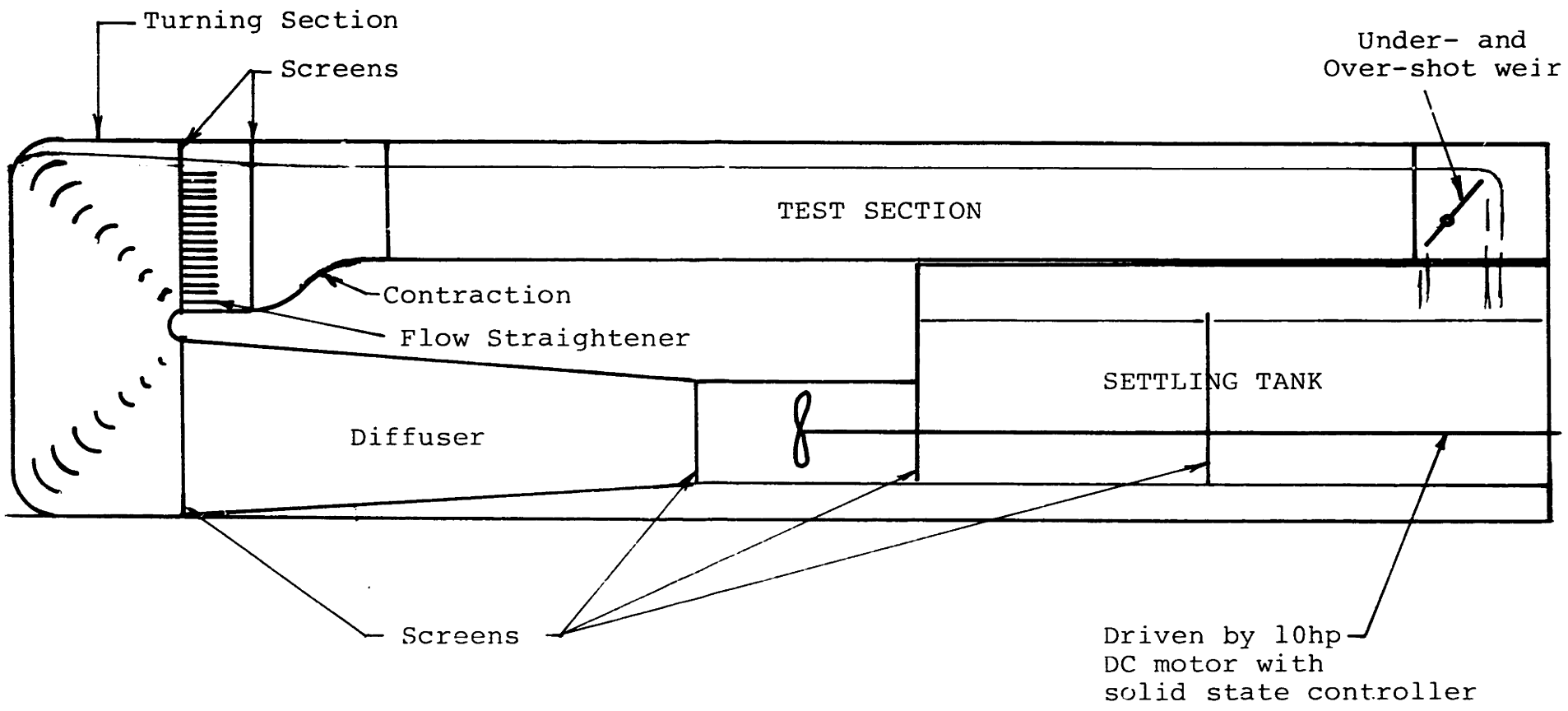

Figure 6.1 Sketch of Precision Flume

position of the weir. All calibrations were done with the settling tank full. Using the resultant data, flow speeds can be determined within approximately 5 percent.

Annemometry

For making velocity surveys a TSI 1050 Series constant temperature annemometer (Models 1051-2D, 1054B, and 1056) was used, equipped with a Model 1231W conical hot film probe. RMS voltages were obtained from a Brüel and Kjoer Model 2416 RMS voltmeter, and a Federal Scientific UA-15A Ubiquitous Spectrum Analyser and 1015 Spectrum Averager were used for spectral analysis.

Oil

Two types of mineral oil were used, of specific gravities .874 and .921, viscosities 14.0 and 150cp, surface tensions 28.6 and 30.8 dynes/cm, and interfacial tensions 39.7 and 47.1 dynes/cm, respectively.

PROCEDURES

Recording of Oil Depths

A barrier extending approximately 6 inches below the free surface was installed across the test section far enough forward

of the weir that the weir did not influence the flow around the barrier. A block of rubberized horsehair 18 inches long by 18 inches wide by 6 inches deep was positioned in front of the barrier in order to prevent the inception of corner vortices, which tend otherwise to entrain oil. The effectiveness of horsehair for this purpose was reported by Hale, Norton, and Rodenberger (1974).

With the flume running at the lowest speed of interest, oil was pumped onto the free surface in front of the barrier. When the oil extended almost the length of the test section, the oil delivery was stopped. The flow was allowed to reach its steady configuration, and the position of the oil-water and oil-air interfaces at various positions were measured by eye through the sides of the test section. The reference position used was that of the free surface in the absence of oil, as previously marked on the side of the test section. The measurements were averaged over a number of periods of flow speed oscillation. At higher flow speeds, where wall effects are noticeable, depths were averaged over the width of the flume. For this reason, the data were somewhat imprecise. The flow speed was increased in steps, adding oil when necessary. Both types of oil were used.

Determination of Interfacial Friction

For this experiment the lighter oil was used, and a flow speed of .55 fps was selected. A small amount of dyed oil was made up by dissolving a few grains of Dupont Oil Blue A in a few ounces of the light oil. This mixture was put in a hypodermic syringe. At various positions along the oil slick a vertical stripe of dye was made, extending from the interface to the free surface. The time it took the ends of the stripe to move apart 2 inches was recorded by a stop watch. This procedure tended to filter out motions due to the flume oscillations, since those motions tend to introduce slug flow in the oil. It was found that diffusion of the dye on the interface obscured to some extent that end of the stripe. Downstream of the headwave the center of the resulting pool of dye was taken to be the relevant position, but on the front of the headwave diffusion was so strong that reliable data was unobtainable. Furthermore, the existence of waves on the lee side of the headwave may have contributed to the drift of the dye.

Nature of the Instability

Heavy oil was placed in the flume at different flow velocities, and the interfacial waves on the lee side of the headwave were observed. Wave lengths were estimated by eye,

and phase velocities were measured by timing an individual wave's transit of a prescribed distance.

Rigid Headwave

Due to the vigorous instability on the lee side of the headwave, it is extremely difficult to measure mean velocity profiles in this region and impossible to measure real turbulence. To avoid these difficulties, a wooden form was made which conformed to the measured mean shape of the heavy oil in a current of .94 fps. This form was placed in the flume at this speed, and the water height adjusted appropriately. Three holes were drilled through the form in the region of interest and the annemometer probe extended through each hole into the flow. Mean voltages were recorded. RMS data were also obtained, but the frequency spectra revealed that convection noise was masking the data.

Rigid Upper Boundary

A plywood cover was constructed which would extend over most of the test section. It was installed in a horizontal position in front of the barrier. The flow height was increased until the cover was just wetted. Heavy oil was introduced, and after it reached equilibrium, the leading edge flow was observed.